Minimum necessary strain to induce tangled dislocation to form cell and grain boundaries in a 6N–Al

Elsevier Editorial System(tm) for Materials Science & Engineering A

Manuscript Draft

Manuscript Number: MSEA-D-19-04324R1

Title: Minimum necessary strain to induce tangled dislocation to form cell and grain boundaries in a 6N-Al

Article Type: Research Paper

Keywords: 6N-Aluminum; Dislocation structure; Cell structure; HPT; strengthening model; nanoindentation.

Corresponding Author: Professor Marcello Cabibbo, PhD

Corresponding Author's Institution: università politecnica delle marche

First Author: Marcello Cabibbo, PhD

Order of Authors: Marcello Cabibbo, PhD

Abstract: Severe plastic deformation (SPD) techniques are known to promote exceptional material properties by inducing significant modifications in the metallic material microstructure. In particular, severe plastic deformation (SPD) techniques are known to effectively refine the initial grain structure of f.c.c. and b.c.c. crystals to sub-micrometre levels. Pure metals are mostly appropriate to study the early stages of the microstructure modifications induced by SPD. This is chiefly due to the possibility to isolate the material strengthening due to dislocations from other possible microstructure features. To this purpose, a high-purity 6N-aluminum (99.9999% purity) was here used to study the minimum necessary strain to form crystal boundaries (that is, cell and grain boundaries). Cell and grain boundaries are formed from previously introduced tangled dislocations (TD), which constitute the microstructure modification features at the early stages of plastic deformation. In this study, the 6N-Al was subjected to high-pressure torsion (HPT) by which the minimum necessary strain, eps_eq, to form cell boundaries was identified. It was thus find that, TD started to evolve to cell boundaries at eps_eq = 0.05. This finding was validated by a second SPD technique, such as accumulative roll bonding (ARB). A microstructure strengthening model was applied and validated by nanoindentation measurements.

Cover letter

The present manuscript entitled: “Minimum necessary strain to induce tangled dislocation to form cell and grain boundaries in a 6N-Al” by Marcello Cabibbo (DIISM / Università Politecnica delle Marche, Via Brecce Bianche 12, 60131 – Ancona, Italy) focuses on early stages of plastic deformation induced in a high-purity aluminum by high pressure torsion (HPT). The objectives and methodologies of the manuscript are within the aims and scopes of the journal. A discussion section deals with a proposed strengthening model also discussed with previously published contributions. These were mostly published in the Materials Science Engineering A journal, as well as some cited publications by this author.

The manuscript is original and no part of it has been published before, nor is any part of it under consideration for publication at another journal. The author also declares no conflicts of interest.

Yours, sincerely,

Prof. Marcello Cabibbo

Replies to the Reviewers' comments:

The author thanks the Reviewer for having improved the understanding of the findings presented in the manuscript by his comments and remarks.
In the following, replies to each of the Reviewers comments are reported.
The manuscript text was modified according to the comments and replies here listed. These modifications are highlighted in yellow in the "marked manuscript text only" file.

Reviewer #1: This work studies the a very critical topic, the minimum strain required to generate grain boundaries via a high concentration of dislocations. This work provides fundamental understanding of an important microscopic phenomenon coupled with mechanical deformation, which is within the scope of MSEA. It is recommended for publication in MSEA, while the following concerns need to be addressed before publication. Also, improvement of the language is required.

Language was improved by proof-reading the manuscript text.

In the following, the Reviewers comments are reported, together with the related replies.

1. *It seems that Figures 1 and 2 can be combined.*
REPLY: Figs 1 and 2 are now combined into Figure 1(a) and 1(b), respectively.

2. *There are networks of dislocations in the grain (e.g., Figure 3h). Are these networks related to the tangled dislocations?*
REPLY: Yes. The showed dislocations within the LABs and HABs of Fig. 3h (now Fig. 2(h)) are actually tangled dislocations that are in the process to reorganize into LABs by the induced shear deformation.
With this respect, the following was added in the manuscript text:
"In particular, starting from the minimum necessary strain $\varepsilon_{eq} \cong 0.05$ to form dislocation boundaries, tangled dislocations (TDs) are continuously formed within the newly formed cell and grain structures. These can be seen also at the maximum strain level here inspected ($\varepsilon_{eq} \cong 0.10$ of Fig. 2h)."

3. *Page 4: "To avoid any possible artefact during sample preparation..." it should be "artifact".*
REPLY: Change made.

4. *The experimental part should be reorganized. Different experimental sections should have their own subtitles.*
REPLY: Experimental section is now reorganized into 4 separated subsections: 2.1. The material; 2.2. High-Pressure Torsion and Accumulative Roll Bonding methods; 2.3. Sample preparation and Transmission electron Microscopy details; 2.4. Nanoindentation methods.

5. *The preparation of TEM sample involves pouching. Will this generate dislocations? Are the low-concentration dislocations in Figure 1 generated by punching?*
REPLY: It is unlikely that the quite few, short, and widely spaced free dislocations showed in Fig. 1(a) could be generated by punching the thin foil to obtain the TEM discs. These few short dislocations are rather believed to originate by a sort of thermal effect during annealing. It is possible that some dislocations of the coarsening grains during annealing are induced to detach from the boundary and remains within the fully recrystallized grained structure. Thence, these few free dislocations could be attributed to a statistical thermal effect of a ultra-purity aluminum in its fully annealing metallurgical state. With this respect, for a sake of clarity, the following sentence was added in the text:
"These few, short and dispersed free dislocations are likely to be generated as statistical phenomenon induced by annealing from the boundaries of the coarsening grains."

6. Are there any TEM observation showing the evolution of tangled dislocations into grain boundaries?
REPLY: The process of TD promotion into cell boundary (*i.e.*, low-angle boundary, LAB) was actually documented by TEM inspections. Fig. 3 (now Fig. 2) now includes a TEM micrograph of the experimental condition $\varepsilon_{eq} \cong 0.05$ showing this process of TD recombination into a LAB. That is, Fig. 2(c) was changed with another showing the initial process of TDs promotion into cell walls.

Although grain boundaries inhibit the movement of dislocations and accumulate them, question remains how the grain boundaries are generated from dislocations?
REPLY: To better explain and discuss the process of cell and grain boundary formation, starting from the tangled dislocations, the following was added.
"Thus, the process of boundary formation from TDs can be described as follow. During shear plastic deformation, the newly formed TDs are induced to accumulate within the grains along specific crystallographic planes and directions. The preferential dislocation glide planes are the Al-[002] and the dislocations mostly accumulate along the Al-(200) directions. TDs tend to accumulate to form series of broad linear zones characterized by long and highly dense dislocations. These, in turns, are induced to evolve into dense dislocation walls (DDWs). Whenever the DDWs are formed the portion of the Al-matrix where they are located is locally deformed and a low misorientation of few tens to 1-1.5° is produced across the wall. This actually indicates that the new lines of DDWs generally represent discontinuities of the crystal uniformity within the aluminum grains. That is, the DDW structures consist of randomly oriented dislocation forming block of line defects that progressively rise their cumulative mean misorientation and get thinner with cumulative shear deformation.
Indeed, it was here shown that at a strain $\varepsilon_{eq} > 0.05$, the misorientation angles across the DDWs increased to a level by which DDWs assume the microstructure and mechanical character of cells, *i.e.* LABs (Fig. 3c). The width of DDWs gradually decrease and, correspondingly, the misorientation angles across DDWs increase progressively during straining. Thus, the formation of the DDWs, during straining, is likely to be due to a local accommodation process of the lattice curvatures at the zones of TD accumulation.
This argumentation is consistent with the analyses and models introduced by Hansen et al. [20]. In their model, they differentiate the TDs possibly forming low-misorientation dislocation lines, named as incidental dislocations (IDs), from the ones having larger misorientation, which are GNDs. These latter are considered the ones equivalent to the DDWs. It seems then that a dislocation substructure hierarchy governs the evolution of TDs to DDWs, occurring at the earlier stages of dislocation recombination to form cells (LABs) and grains (HABs). This process occurs above a specific local dislocation saturation limit. Thence, GNBs are the portion of free dislocations responsible for the formation of the cell and grain structure upon plastic deformation. In fact, at the site of the forest TDs forming DDWs, local lattice rotations is generated by excess dislocation density, which are always characterized by deformation-induced lattice rotations and long-range internal stresses. This microstructure evolution process indicates that the TD agglomerates that are induced by the plastic deformation are indeed dislocation walls (DWs) [20]. On the other hand, IDs are statistically formed free dislocation lines that move across the crystal under the effect of the external load. These are mobile line defects with minimal capability to form thick dislocation agglomerations. That is, from a statistical viewpoint IDBs do not contribute to form DDWs. On the contrary, GNDs are induced to accumulate and to form alternating misorientation angles depending on the different followed slip systems under external load [21].
Finally, the presence of grain boundaries, both the new and the ones formed on annealing can hinder the formation of wall-like structures. In fact, the grain boundary not only acts as an obstacle to dislocation motion, but also affects the resulting dislocation stress field. On the other hand, the crystallographic mismatch across a grain boundary is likely to accelerate the emission away or absorption into the boundary line of dislocations. In the present case, the initial 6N-Al annealing state consisted of quite wide grained-structure with grain size higher than 100 □m. Thus, the resulting wide grain boundary network had a limited hindering effect on the generation of TDs and eventual formation of DDWs during the early stages of plastic deformation."

Minimum necessary strain to induce tangled dislocation to form cell and grain boundaries in a 6N-Al

Marcello Cabibbo

DIISM / Università Politecnica delle Marche, Via Brecce Bianche 12, 60131 – Ancona, Italy.

Keywords: 6N-Aluminum; Dislocation structure; Cell structure; HPT; strengthening model; nanoindentation.

Abstract. Severe plastic deformation (SPD) techniques are known to promote exceptional material properties by inducing significant modifications in the metallic material microstructure. In particular, severe plastic deformation (SPD) techniques are known to effectively refine the initial grain structure of *f.c.c.* and *b.c.c.* crystals to sub-micrometre levels. Pure metals are mostly appropriate to study the early stages of the microstructure modifications induced by SPD. This is chiefly due to the possibility to isolate the material strengthening due to dislocations from other possible microstructure features. To this purpose, a high-purity 6N-aluminum (99.9999% purity) was here used to study the minimum necessary strain to form crystal boundaries (that is, cell and grain boundaries). Cell and grain boundaries are formed from previously introduced tangled dislocations (TD), which constitute the microstructure modification features at the early stages of plastic deformation. In this study, the 6N-Al was subjected to high-pressure torsion (HPT) by which the minimum necessary strain, ε_{eq}, to form cell boundaries was identified. It was thus find that, TD started to evolve to cell boundaries at ε_{eq} = 0.05. This finding was validated by a second SPD technique, such as accumulative roll bonding (ARB). A microstructure strengthening model was applied and validated by nanoindentation measurements.

1. Introduction

In the last few decades, thermally stable ultrafine-grained (UFG) metallic materials and alloys were widely studied and characterized as they showed superior mechanical properties compared to the conventional grained counterparts [1]. With this respect, a number of grain refining methods were proposed and developed so far. In particular, top-down approaches, such as severe plastic deformation (SPD) are the ones showing the most promising and technologically reliable techniques to obtain sound UFG metals [2-4].

To understand the physical principles behind the SPD-driven UFG formation, pure metals are typically used. In particular, pure aluminum has a relatively low melting temperature (933 K) and a high stacking fault energy (γ_{SFE} = 166 mJ·m^{-2}). Pure Al, with different purity levels, was the referee metallic material used for a variety of fundamental studies involving all the most relevant SPD techniques. These include high-pressure torsion (HPT), equal-channel angular pressing (ECAP), accumulative roll-bonding (ARB), accumulative press-bonding (APB), twist extrusion (TE), friction stir processing (FSP), cyclic extrusion-compression (CEC), repetitive corrugation and straightening (RCS), accumulative back extrusion (ABE) and hydrostatic extrusion (HSE), high-pressure sliding (HPS) ([4-6] and references therein).

It is thus now widely recognized that the exceptional mechanical properties achieved by the UFG metals can be attributed to both the sub-micron cell, grain size and the mobile dislocations within grains. The evaluation of the tangled dislocations (TD) density is thus an important microstructure feature to understand the evolution from conventional-grained to UFG under SPD. Several published works [4-10] recognized that the UFG formation proceeds from TD and dense

dislocation walls (having very low-angle boundaries), which are continuously introduced in the material during SPD, and that eventually rearrange to form cell structures (low-angle boundaries, LABs). These latter are in turns induced to increase their misorientation angle to eventually become grain boundaries (high-angle boundaries, HABs). With this respect, the identification of the minimum necessary SPD strain to promote the newly introduced TD to form cell boundaries is an important issue for the UFG production processes.

The present study focused on the microstructure TEM-based determination of the minimum necessary strain to promote the formation of cell, and eventually grain boundaries, from tangled dislocations in a high-purity 99.9999% (6N-Al) aluminum. To this purpose, the 6N-Al was subjected to HPT, and eventually to ARB to double-check the results obtained by HPT.

HPT was used as it allows characterizing the early stages of shear plastic deformation induced in the material. In fact, HPT generates progressive plastic deformation levels from a minimum at the disc center, to a maximum at the disc periphery. The level of induced strain strongly depends on the number of HPT rotations, *N*. In HPT, the sample, in form of a thin disc, is placed between two large anvils and subjected to a high pressure and concurrent torsional straining. This way, the two meaningful parameters are the magnitude of the imposed pressure, *P*, and the number of revolutions applied to the sample, *N*. The imposed strain chiefly depends on the distance from the disc center, and thus the microstructure modifications imposed by HPT are greatly inhomogeneous by a continuous rate from disc periphery to its center. For the present study, this latter aspect is considered as a key microstructure aspect to determine the minimum necessary strain level to form cell boundaries by TD rearrangement. In this sense, HPT is different from most SPD processes, such ECAP, TE, or FSP, where strain gradients are generated quite quickly making almost impossible to determine the early stages of cell structure formation.

2. Experimental procedures and Method

2.1. The material

A 6N-Al (purity of 99.9999%) was used for this study. The 6N-Al was fully annealed at 655 K / 60 min. As shown in Figure 1(a), the annealed aluminum showed a coarse-grained structure with quite few free dislocations within the grains. These few, short and dispersed free dislocations are likely to be generated as statistical phenomenon induced by annealing from the boundaries of the coarsening grains.

2.2. High-Pressure Torsion and Accumulative Roll Bonding methods

The annealed 6N-Al was subjected to HPT at different experimental conditions, to obtain an almost continuous range of strain levels, *i.e.*, from ε_{eq} = 0.02-to-0.24. Figure 1(b) is a schematic representation of the HPT strain deformation imposed to a typical disc sample. The incremental shear strain is given by $d\omega/\omega$, being ω the angular rotation around the disc center. The equivalent vön Mises strain imposed by HPT is calculated according to [11], Eq. (1a):

$$\varepsilon = \frac{2}{\sqrt{3}} ln\left[\left(\frac{1+\gamma^2}{4}\right)^{0.5} + \frac{\gamma}{2}\right] \qquad \text{Eq. (1a)}$$

where $\gamma = (2\pi Nr)/t$ is the shear strain, r the distance from the disc center, ranging from 0 to R (disc radius), t the disc thickness. From Eq. (1a), the equivalent strain, ε_{eq}, variation with the distance to disc center is:

$$\varepsilon_{eq} = \frac{2\pi N r}{t\sqrt{3}}$$ Eq. (1b)

The initial disc radius, *R*, and thicknesses, *t*, were 20 mm and 1 mm, respectively. HPT was carried out at room-temperature by depressing the vertical anvils to a depth of 0.05 mm. Torsion strain was exerted by rotating the upper anvil at a low rotation speed of 0.17 rpm ($1°sec^{-1}$) under a pressure of 38 MPa (300 Kg load). In order to apply low rates of strain, the number of rotation were reduced to *N* = 1/120, 1/72, and 1/45. The disc flowed to the radial direction during HPT due to the lack of side constraint, resulting in a thickness reduction almost irrelevant, being, respectively, ~0.05, ~0.05, and ~0.06 mm, from the initial 1 mm disc thickness. TEM inspections were performed at the mid-section of the discs (that is, at a thickness $t \cong 0.5$ mm) at different distances from the disc center: ~0.3, ~0.6, ~0.9, ~1.2, and ~1.5 mm. The resulting equivalent strains, ε_{eq}, were calculated by Eq. (1b) and are listed in Table 1.

The reason to use HPT to perform the present study is based on the possibility to generate an almost continuous incremental strain level, starting form a minimum equivalent strain level as low as $\varepsilon_{eq} = 0.02$.

	distance to disc center, *r*, mm				
angular rotation, θ, °	~0.3	~0.6	~0.9	~1.2	~1.5
5 (*N*=1/120)	0.02	0.04	**0.05**[1]	0.07	0.09
10 (*N*=1/72)	0.03	0.06	0.09	0.12	0.15
15 (*N*=1/45)	**0.05**[1]	0.10	0.14	0.19	0.24

Table 1. Equivalent strain, ε_{eq}, obtained by HPT *N* = 1/120, 1/72, and 1/45 turns, and *r* = 0.3, 0.6, 0.9, 0.12, and 0.15 mm from disc center. Bold values refer to the performed TEM inspections. The $\varepsilon_{eq}{}^{1} = 0.05$ is the minimum necessary strain to form cell boundaries from TD in 6N-Al.

Yet, to double-check the soundness of the experimental results obtained by HPT, the annealed 6N-Al was also subjected to ARB at the same minimum strain level found by HPT to start forming cell/grain boundaries from TDs.

ARB was carried out on two equally-thick annealed 6N-Al strips to make a stacked thickness of 1 mm. These were roll bonded at room temperature to a 3% thickness reduction. A second round of ARB with same 3% thickness reduction was also performed. This way, the 6N-Al was subjected to a vön Misses equivalent strain of, respectively, ε_{eq} ~0.05, and ε_{eq} ~0.10. The rolls diameter were 80 mm and the roll peripheral speed was about 60 mm/min.

2.3. Sample preparation and Transmission electron Microscopy details

To avoid any possible artifact during sample preparation, the ~1 mm-thick HPT processed discs were prepared for TEM inspections by chemical and electro-chemical means only. They were punched to 3 mm TEM discs at HPT positions indicated in Figure 1(b). The 3 mm-wide and ~1 mm-thick TEM discs were chemically thinned to ~200 μm using a solution of 15% HCl_4, 15% $C_3H_3(OH)_3$, 70% methanol. Finally, they were electro-chemically polished to electron transparency by double-jet with a solution of 1/3 nitric acid and 2/3 methanol at 238 K and V = 12V. TEM inspections were carried out using a Philips™ C-20® working at 200 keV with a double-tilt specimen holder equipped with a liquid-nitrogen cooling stage. Inspections were performed at the middle height of the HPT discs. Same procedures were followed to prepare the ARB TEM discs. In this latter case, discs were extracted along the ARB strip section and observations were carried out at the central zone of the two bonded strips.

Two-beam excitation conditions were selected for most of the TEM observation and dislocation characterizations. Tangled dislocation (TD) density, ρ_{TD}, was quantified using Ham's interception stereological methods [12]. Thence, ρ_{TD} was calculated through the count of interception points

between the mesh and the existing dislocations, n_{disl}, in the TEM micrographs. This was evaluated by $\rho_{TD} = 2n_{disl}/(l_{mesh}t_{TEM})$, were, l_{mesh} is the total length of the mesh, and t_{TEM} is the thickness of the TEM foil. Crystal thickness, t_{TEM}, was determined through the diffracted beam intensity variation under dual beam conditions, using converged electron beam diffraction (CBED) patterns. This way, by plotting the linear interpolation of data points in a $S^2/n_{fringes}^2$ vs. $n_{fringes}^{-2}$ graph, where S is the fringes spacing and $n_{fringes}$ the number of counted fringes, t_{TEM}^{-2} was determined at y-axis line intercept. The error due to the invisible dislocations (i.e., the ones oriented as to have $b \cdot g = 0$, where b is the Burgers vector and g refers to the dislocation lying crystallographic plane) is within the experimental error of the foil thickness evaluation. Cell (LAB) and grain boundary (HAB) misorientation were measured by Kikuchi band patterns. The misorientation angle measurement procedure by Kikuchi pattern on TEM is fully described elsewhere in previous published works by this author [7,8]. All TEM inspections were carried out by orienting the aluminum matrix [002] crystallographic plane parallel to the electron beam.

2.4. Nanoindentation methods

Nanoindentation measurements were performed at same HPT disc height as TEM inspections. For the nanoindentation measurements, samples were prepared by the same chemical thinning methods used for the TEM foil preparation. A Hysitron™ Triboscope UBI-1® was used. Calibration procedures were followed according to [13]. A trapezoidal load function of 5 s loading, 15 s at the set load, and 5s unloading was used, with a set load of 1000 μN. The reported data were averaged over a series of 4 8x8 matrix of individual measurements spaced 250 μm. Data analysis was performed according to the Oliver-Pharr method [14].

3. Experimental Results

The plastically deformed 6N-Al HPT microstructure at different HPT experimental conditions is reported in Figure 2. The Figure reports representative TEM micrographs taken at N = 1/120, r = 0.3 (Fig. 2a), 0.6 (Fig. 2b), 0.9 (Fig. 2c), 1.2 (Fig. 2d), 1.5 mm (Fig. 2e), at N = 1/72, r = 0.9 (Fig. 2f), at N = 1/45, r = 0.3 (Fig. 2g), and r = 0.6 mm (Fig. 2h). It appears that at the lowest strain levels ($\varepsilon_{eq} < 0.05$) the plastically deformed microstructure is only constituted by TDs, which have quite low dislocation density at $\varepsilon_{eq} = 0.02$ (Fig. 2a). These are induced to group with the strain. The ρ_{TD} values obtained at the different TEM inspected HPT conditions are listed in the Table 2. It resulted that, ρ_{TD} steadily increased from $\varepsilon_{eq} = 0.02$ to 0.05, to eventually slightly decrease at $\varepsilon_{eq} > 0.07$, in favour of the early formation of dislocation boundaries (*i.e.* cell boundaries). In fact, TEM inspections (Figs. 2e, f, h) clearly showed that at $\varepsilon_{eq} \cong 0.05$ cell boundaries started to form. At ε_{eq} = 0.09-0.10 some grain boundaries (HAB) were also detected (Fig. 2h). In particular, starting from the minimum necessary strain $\varepsilon_{eq} \cong 0.05$ to form dislocation boundaries, tangled dislocations (TDs) are continuously formed within the newly formed cell and grain structures. These can be seen also at the maximum strain level here inspected ($\varepsilon_{eq} \cong 0.10$ of Fig. 2h). This in turns means that the minimum necessary strain to induce the formation of cell, and eventually grain boundaries, can be identified as $\varepsilon_{eq} \cong 0.05$. That is, the initiation of microstructure refining process induced by the plastic deformation can be identified at a strain of $\varepsilon_{eq} \cong 0.05$. It is noteworthy that the dislocation densities here reported are quite low and this is likely to be due to the small strain applied to the 6N-aluminum.

The results obtained by HPT process were also verified by ARB. Figure 3 shows representative TEM micrographs of the microstructure at ARB ε_{eq} ~0.05 (Fig. 3a) and ε_{eq} ~0.10 (Fig. 3b). It appeared that at ARB ε_{eq} ~0.05 no cell boundary formation were detected. This actually confirmed the soundness of the conclusions drawn by HPT. These experimental results seem to confirm that

ε_{eq} ~0.05 was the minimum necessary strain to form cell, and eventually grain boundaries in high-purity aluminum. This in turns mean that the UFG process starts to activate from a minimum strain level of ε_{eq} ~0.05 in SPD pure aluminum. The fine-grained structure formation is actually activated whenever a crystal region containing TDs is subjected to a sufficient strain gradient to induce ρ_{TD} rises as to eventually reach a critical (threshold) value. Above this threshold-like strain level, these dislocations start to commonly group to a certain crystallographic orientation, thus forming a cell wall (LAB). Under the effect of the shear deformation, LABs are induced to evolve into cell boundaries, and eventually to grain boundaries (HABs).

	ε_{eq}							
	0.02 *N*=1/120, *r* = 0.3 mm	0.04 *N*=1/120, *r* = 0.6 mm	0.05 *N*=1/120, *r* = 0.9 mm	0.05 *N*=1/45, *r* = 0.3 mm	0.07 *N*=1/120, *r* = 1.2 mm	0.09a *N*=1/120, *r* = 1.5 mm	0.09b *N*=1/72, *r* = 0.9 mm	0.10 *N*=1/45, *r* = 0.6 mm
ρ_{TD}, 10^{12} m^{-2}	3	18	235	180	160	55	86	62

Table 2. TD density, ρ_{TD}, measured at different strain levels, ε_{eq}, from ε_{eq} = 0.02 to 0.10.

4. Discussion

The here obtained microstructure results suggested a sort of correlation between the minimum necessary strain to initiate cell boundaries (LABs) formation and the amount of TDs that are generated during the plastic deformation. In fact, it was found that the TD density steadily increased with strain up to the strain level where cells and grains started to form. Starting from this strain level, the density of TDs, $\rho_{TD,}$ slightly reduced (Table 2). On one hand, this is chiefly due to a dislocation annihilation driven by dynamic recovery, due to the low melting temperature and high SFE of the 6N-Al. On the other hand, the $\rho_{TD,}$ reduction is due to the process of TD conversion to cell and grain boundaries, so to reduce the number density of dislocations within the cells and grains. These findings are in good agreement with other previously reported data [15].

The TD rearrangement, driven by the early stages of plastic deformation, is the microstructure process actually responsible for the grain refining process induced by both HPT and ARB. In fact, a large fraction of cell boundaries (LABs) evolving into grain boundaries (HABs) might migrate [16] or dissolve [17]. The cell boundary migration proceeds as collective movement of dislocation boundary perpendicular to the boundary plane. Cell boundary dissolution usually balance the number of cell boundary continuously formed from TDs. This in turns preserve the number fraction of the LABs during the early stages of UFG formation under SPD.

The fraction of TDs able to migrate are usually called geometrically necessary dislocations (GNDs) [15,18,19]. These accommodate strain gradients in non-homogeneous deformation proportionally to the strain gradient. GNDs are hard to annihilate since they statistically have the same sign associated with the direction of strain gradient. Another fraction of TDs is statistically stored by homogeneous deformation, and these are generally called statistically stored dislocations (SSDs) or incidental dislocations (IDs) [18-20]. They are likely to annihilate due to the balance of equal number of different sign dislocations randomly distributed within the crystal [18]. Thus, due to the high SFE of high-purity aluminum, microstructure evolution occurs by TD rearrangement at low levels and low deformation rates under HPT, as high strain levels are needed to achieve microstructural homogeneity. In particular, due to the specific strain path induced by HPT, the vast majority of dislocations, if not all of them, are GNDs [17].

Thus, the process of boundary formation from TDs can be described as follow. During shear plastic deformation, the newly formed TDs are induced to accumulate within the grains along specific crystallographic planes and directions. The preferential dislocation glide planes are the Al-[002] and the dislocations mostly accumulate along the Al-(200) directions. TDs tend to accumulate

to form series of broad linear zones characterized by long and highly dense dislocations. These, in turns, are induced to evolve into dense dislocation walls (DDWs). Whenever the DDWs are formed, the portion of the Al-matrix where they are located is locally deformed and a low misorientation of few tens to 1-1.5° is produced across the wall. This actually indicates that the new lines of DDWs generally represent discontinuities of the crystal uniformity within the aluminum grains. That is, the DDW structures consist of randomly oriented dislocation forming block of line defects that progressively rise their cumulative mean misorientation and get thinner with cumulative shear deformation.

Indeed, it was here shown that at a strain $\varepsilon_{eq} > 0.05$, the misorientation angles across the DDWs increased to a level by which DDWs assume the microstructure and mechanical character of cells, *i.e.* LABs (Fig. 3c). The width of DDWs gradually decrease and, correspondingly, the misorientation angles across DDWs increase progressively during straining. Thus, the formation of the DDWs, during straining, is likely to be due to a local accommodation process of the lattice curvatures at the zones of TD accumulation.

This argumentation is consistent with the analyses and models introduced by Hansen *et al.* [20]. In their model, they differentiate the TDs possibly forming low-misorientation dislocation lines, named as incidental dislocations (IDs), from the ones having larger misorientation, which are GNDs. These latter are considered the ones equivalent to the DDWs. It seems then that a dislocation substructure hierarchy governs the evolution of TDs to DDWs, occurring at the earlier stages of dislocation recombination to form cells (LABs) and grains (HABs). This process occurs above a specific local dislocation saturation limit. Thence, GNBs are the portion of free dislocations responsible for the formation of the cell and grain structure upon plastic deformation. In fact, at the site of the forest TDs forming DDWs, local lattice rotations is generated by excess dislocation density, which are always characterized by deformation-induced lattice rotations and long-range internal stresses. This microstructure evolution process indicates that the TD agglomerates that are induced by the plastic deformation are indeed dislocation walls (DWs) [20]. On the other hand, IDs are statistically formed free dislocation lines that move across the crystal under the effect of the external load. These are mobile line defects with minimal capability to form thick dislocation agglomerations. That is, from a statistical viewpoint IDBs do not contribute to form DDWs. On the contrary, GNDs are induced to accumulate and to form alternating misorientation angles depending on the different followed slip systems under external load [21].

Finally, the presence of grain boundaries, both the new and the ones formed on annealing can hinder the formation of wall-like structures. In fact, the grain boundary not only acts as an obstacle to dislocation motion, but also affects the resulting dislocation stress field. On the other hand, the crystallographic mismatch across a grain boundary is likely to accelerate the emission away or absorption into the boundary line of dislocations. In the present case, the initial 6N-Al annealing state consisted of quite wide grained-structure with grain size higher than 100 μm. Thus, the resulting wide grain boundary network had a limited hindering effect on the generation of TDs and eventual formation of DDWs during the early stages of plastic deformation.

To verify the soundness of the results obtained by the TEM microstructure inspections, a strengthening model was also applied. This model included all the meaningful microstructure features. Thus, the 6N-Al yield stress, σ_y, was determined both by linearly adding the microstructure terms, and by hardness measurements by nanoindentation. The microstructure strengthening model was determined as, Eq. (2a):

$$\sigma_y = \sigma_0 + \sigma_{Dislocations} = \sigma_0 + \sigma_{TD} + (\sigma_{VLAB} + \sigma_{LAB} + \sigma_{GB}) \qquad \text{Eq. (2a)}$$

where σ_0 = 10 MPa is the frictional stress of pure Al [**7**], σ_{TD} the stress due to the TDs, σ_{VLAB} the contribution form the cell boundaries with misorientation angle within 2° (very-low angle boundaries, VLABs), σ_{LAB} and σ_{GAB} the contribution coming from the cell (LAB) and grain (HAB) boundaries, respectively. This strengthening model was first introduced by Hansen and the Risø

group accounting for contributions coming from TDs, LABs, and HABs [19]. A more recent strengthening model, reported by the present author in [7], also included the strengthening contribution coming from VLAB (θ_{mis} <2°). According to the TEM observations, for strain levels ε_{eq} < 0.05, the yield stress is expected to be limited to, Eq. (2b):

$$\sigma_y|_{\varepsilon<0.05} = \sigma_0 + \sigma_{TD} \quad \text{Eq.(2b)}$$

On the other hand, at ε_{eq} = 0.05-0.15, Eq. (2) can be rewritten as, Eq. (2c):

$$\sigma_y(\varepsilon=0.05\text{-}0.15) = \sigma_0 + \sigma_{TD} + (\sigma_{VLAB} + \sigma_{LAB}) \quad \text{Eq.(2c)}$$

According to [22,23], being the TDs essentially coincident with the GNDs ($\rho_{TD} \cong \rho_{GND}$), σ_{TD} can be calculated as, Eq. (3):

$$\sigma_{TD} = M\alpha Gb\rho_{TD}^{0.5} \quad \text{Eq.(3)}$$

where M = 2.94 is the Taylor factor [24,25], α is a fitting constant ranging 0.2-0.3, and usually agreed to be 0.24 [6,18,25,26], G = 26 GPa is the shear modulus of aluminum, and b = 0.286 is the aluminum Burgers vector.

Since at low strain levels, *i.e.* ε_{eq} < 0.10 the detected volume fraction of the cell boundaries was quite low, and that of the grain boundaries was even lower, the strengthening contribution of these could be estimated by taking into account the mean dislocation density forming those boundaries. Thus, according to Hansen *et al.* [18], the following relationships were taken into account, Eq. (4a):

$$\sigma_{VLAB} + \sigma_{LAB} = \sigma_{VLAB+LAB} = M\alpha Gb\rho_{VLAB+LAB}^{0.5} \quad \text{Eq.(4a)}$$

where $\rho_{VLAB+LAB}$ is the average dislocation density that form the very-low angle and low-angle boundaries. These are here considered together, since in the early stages of cell boundary formation from TDs, the misorientation angle was found to be within 8°, with a large fraction of boundary misorientation ranging 2-to-6°.

Anyway, the approach of Eq. (4a) typically holds for a network of boundaries typical of refined or mixed cell/grained microstructures. In the present case, for strains 0.05 < ε_{eq} < 0.10, the volume fraction of cell boundaries, and even grain boundaries, was found to be quite low. That is, the newly formed boundaries are rather scattered in the 6N-Al microstructure. These boundaries have mostly low misorientation angles with few dislocations forming the boundary lines. Thus, to evaluate the cell boundary contribution the approach proposed by Starink and co-workers [22,27,28] was here taken into account, Eq. (4b):

$$\sigma_{VLAB+LAB} = (\alpha' GbS/4.365)\rho_{VLAB+LAB} \quad \text{Eq.(4b)}$$

where α' = 2 [28,29], S is the average distance between the boundary dislocations. This relationship holds for the LABs strengthening contribution.

According to [27,30], the strengthening contribution given by the few grain boundaries that were formed at 0.07 <ε_{eq} < 0.10, was modelled as, Eq. (5):

$$\sigma_{HAB} = \left(\frac{\alpha' Gb}{4.365}\right)\frac{b\rho_{HAB}}{arctg(b/S)} \quad \text{Eq.(5)}$$

Thus, Eq. (2b) and Eq. (2c) become Eq. (6a) and Eq. (6b), respectively:

$$\sigma_y|_{\varepsilon<0.05} = \sigma_0 + M\alpha Gb\rho_{TD}^{0.5} \quad \text{Eq.(6a)}$$

$$\sigma_y|_{\varepsilon>0.05} = \sigma_0 + M\alpha Gb\rho_{TD}^{0.5} + (\alpha' GbS/4.365)\rho_{VLAB+LAB} + \left(\frac{\alpha' Gb}{4.365}\right)\frac{b\rho_{HAB}}{arctg(b/S)} \quad \text{Eq.(6b)}$$

The average distance S of, respectively, LAB, Eq. (4b), and HAB, Eq. (5), was evaluated by TEM inspections. Figure 4 shows a representative TEM micrograph from which these measurements were carried out.

Table 3 reports the 6N-Al yield stress as determined by the Eq. (6a) and Eq. (6b) for the lower strain levels, *i.e.* $\varepsilon_{eq} < 0.10$.

	ε_{eq}							
	0.02 *N*=1/120, *r* = 0.3 mm	0.04 *N*=1/120, *r* = 0.6 mm	0.05 *N*=1/120, *r* = 0.9 mm	0.05 *N*=1/45, *r* = 0.3 mm	0.07 *N*=1/120, *r* = 1.2 mm	0.09a *N*=1/120, *r* = 1.5 mm	0.09b *N*=1/72, *r* = 0.9 mm	0.10 *N*=1/45, *r* = 0.6 mm
σ_{TD}, MPa	9	22	26	22	21	13	17	15
$\sigma_{VLAB+LAB}$, MPa	-	-	6	5	9	11	8	14
σ_{HAB}, MPa	-	-	-	-	-	4	5	11
σ_y, MPa	**19**	**32**	**42**	**37**	**40**	**38**	**40**	**50**

Table 3. Proof stress, σ_y, and individual microstructure contributions (σ_{TD}, $\sigma_{VLAB+LAB}$, σ_{HAB}) as determined by Eq. (6a) and Eq. (6b).

From strain levels $\varepsilon_{eq} > 0.15$, as the strain rises, the cell and grain boundaries increased steadily. Thus, the aluminum microstructure develops a significant volume fraction of cell and grain boundaries. In particular, for a strain level $\varepsilon_{eq} > 0.20$, the microstructure can be already considered as a fine-grained structure characterized by both cell and grain boundary networks. Thence, for these strain levels, the following strengthening model is likely to be the appropriate approach, Eq. (7) [**6,7**]:

$$\sigma_y|_{\varepsilon>0.20} = \sigma_0 + M\alpha Gb\rho_{TD}^{0.5} + M\alpha G[(3b\theta_{LAB}((1-f_{HAB})/d_{LAB}))^{0.5} + k_{HP}(f_{HAB}/d_{HAB})^{0.5}] \quad \text{Eq.(7)}$$

Figure 5 shows the fine-grained microstructure of the 6N-Al as obtained by the maximum strain level of $\varepsilon_{eq} = 0.24$ obtained by HPT (N = 1/45, r = 1.5 mm). The microstructure appeared composed by TDs, cells and grains. This is indeed a typical sub-micrometre microstructure generated by HPT or similar SPD techniques. The 6N-Al yield stress obtained for $\varepsilon_{eq} = 0.24$ by Eq. (7) was σ_y = (105 ± 15) MPa. In fact, at this strain level, the fraction of HAB was less than 0.15%, with mean cell size d_{LAB} = 2.8 μm and mean misorientation θ_{LAB} = 7°. Thus, the contribution given by the TD was σ_{TD} = 38 MPa, the one given by the cells was $\sigma_{LAB} \cong$ 62 MPa, and the one given by the few grains was $\sigma_{HAB} \cong$ 5 MPa.

This TEM-based microstructure approach was verified by mechanical tests, using nanoindentation measurements. To this purpose, the applied load was the minimum possible according to the specific calibration procedure here followed (see [13], for further details). Indentation load was thus P = 1000 μN, since even lower loads would generate a significant scatter of hardness data that would have jeopardize the readability of the obtained results. By applying a load P = 1000 μN a mean experimental error of ~10% was obtained. Figure 6(a) shows

nanoindentation load-displacement curves for ε_{eq} = 0.02-to-0.10, referring to the HPT experimental conditions highlighted in bold numbers in Table 1 (the ones experimentally inspected by TEM).

A linear relationship holds between hardness, H_V, and yield stress, given by $H_V = (\sigma_y/3)\cdot(0.1)^{m-2}$, where m is the Meyer's hardness coefficient [31]. In the aluminum cold-rolled and annealed metallurgical status, this relationship reduces to $H_V = \sigma_V/\chi$, where χ =2.9-2.8 [6,30-33]. Moreover, the nanoindentation hardness ($H_{nanoind}$) can be converted into H_V by a factor of 0.0945, that is $H_V = 0.0945\cdot H_{nanoind}$ [32]. Thus, to correlate the results obtained by the microstructure model of Eqs. (6a) and (6b), two curves were plotted in Figure 6(b). A first curve refers to the measured nanoindentation hardness $H_{nanoind}$; a second curve refers to the quantity $\sigma_y/(2.9\cdot0.0945)$ both plotted as a function of the strain level, ε_{eq}. The quantity $\sigma_y/(2.9\cdot0.0945)$ represents the expected hardness measured by nanoindentation $H_{nanoind}^{exp}$, where σ_y is determined by the TEM microstructure analyses and the applied strengthening model.

It resulted that the measured, $H_{nanoind}$, and the calculated, $H_{nanoind}^{exp}$, hardness trends with equivalent strain were quite similar, this latter appearing constantly below the $H_{nanoind}$ curve. That is, the nanoindentation measurements were able to confirm the soundness of the microstructure-based approach here reported. In fact, the measured hardness, $H_{nanoind}$, essentially followed the same trend of the $H_{nanoind}^{exp}$ that was obtained by the microstructure-based model. On the other hand, the hardness overestimation by the nanoindentation direct measurements is likely to be due to a local hardening effect of the Berkovich tip. Even if the applied load was quite low (P = 1 mN), a small offset of the hardness reading can be generated. This is most likely due to a certain amount of aluminum hardening generated by holding the tip in contact to the soft material during the measurements. The tip contact holding time was fixed at 15 s, and lower times would have made the loading curves virtually non-reliable, due to the large amount of instrumental transducer noise. As a matter of fact, also the nanoindentation hardness measurement of the ε_{eq} = 0.24 (HPT, N = 1/45, r = 1.5 mm) experimental condition showed values slightly higher than the ones obtained by converting the obtained yield stress to equivalent hardness, $H_{nanoind}^{exp}$ (ε_{eq} = 0.24) (Fig. 6(b)).

The occurrence of 6N-Al hardening under Berkovich tip contact was verified by tuning the dwelling time of the trapezoid load function. That is, a series of indentation at different dwelling times, t_{dwell} = 5, 10, 15, 20, 30, 60, 90, 120, 180 s, and same load-unload rates of 1 mN/5s were carried out in the sample at ε_{eq} = 0.24 (HPT, N = 1/45, r = 1.5 mm) condition. To this purpose, 5 different measurements were performed at each of the set t_{dwell}. Figure 7 reports the mean hardness obtained over the 5 individual measurements at the different set t_{dwell}. It appeared that, for t_{dwell} = 5 and 10 s the hardness values are rather scattered and fuzzy, jeopardizing the actual evaluation of the data. At t_{dwell} = 15 and 20 s, the discrepancy between the measured values and the ones calculated by the strengthening model is of ~20 MPa. For dwelling times $20 < t_{dwell} < 90$ s, the discrepancy tended to saturate to the amount obtained already at t_{dwell} = 15 and 20 s. For $t_{dwell} \geq 90$ s, the measured hardness started to further deviate from the calculated value. As already reported by Cabibbo *et al.* in [34], and as expected by the references therein, this further deviation is due to a room-temperature creep phenomenon to which aluminum is subjected under constant tip load. Thence, the data reported in Figure 7 well explain that the overestimation of the hardness by nanoindentation, compared to the hardness values obtained by the microstructure-based model, is likely to be attributed to a tip load material hardening mechanism.

5. Conclusions

In this study, the early stages of plastic deformation in high-purity 6N-aluminum were investigated by high-pressure torsion (HPT) technique. HPT allowed to characterize the microstructure modification and evolution for quite low strain levels, ε_{eq} = 0.02-to-0.24. HPT

results were validated by a SPD ARB technique. A strengthening model also validated the microstructure findings.
The following conclusions can be outlined.

a. A minimum necessary strain level to promote the boundary formation (low-angle boundaries) starting from tangled dislocations was determined as $\varepsilon_{eq} \sim 0.05$.
b. A strengthening model was applied to identify the microstructure features contributing to the aluminum strengthening induced by the early stages of plastic deformation.
c. To validate the soundness of the obtained results by TEM inspections and the related strengthening model, nanoindentation measurements were carried out at the lowest possible load of 1000 μN were performed. Experimental data followed quite closely the calculated hardness obtained applying the strengthening model. In particular, the nanoindentation hardness values were constantly higher than the values derived from the strengthening model.
d. The nanoindentation data overestimation was found to be most likely due to a tip load hardening effect occurring during the nanoindentation tests.

Acknowledgements: The author is grateful to "Istituto Sperimentale Metalli Leggeri" of Novara for the 6N-Al material delivery. Mr. M. Pieralisi is acknowledged for the HPT tests.

References

[1] X.X. Huang, N. Hansen, N. Tsuji, Hardening by annealing and softening by deformation in nanostructured metals, Science 312 (2006) 249-251.
[2] I.A. Ovid'ko, R.Z. Valiev, Y.T. Zhu, Review on superior strength and enhanced ductility of metallic nanomaterials, Prog. Mater. Sci. 94 (2018) 462-540.
[3] M. Cabibbo, Nanostructured Cobalt Obtained by Combining Bottom-Up and Top-Down Approach, Metals 8(11) (2018) 962-971.
[4] I. Sabirova, M.Yu. Murashkin, R.Z. Valiev, Nanostructured aluminium alloys produced by severe plastic deformation: New horizons in development Mater. Sci. Eng. A 560 (2013) 1-24.
[5] Y. Ito, K. Edalati, Z. Horita, High-pressure torsion of aluminum with ultrahigh purity (99.9999%) and occurrence of inverse Hall-Petch relationship, Mater. Sci. Eng. A 679 (2017) 428-434.
[6] M. Cabibbo, Microstructure strengthening mechanisms in different equal channel angular pressed aluminum alloys, Mater. Sci. Eng. A560 (2013) 413-432.
[7] M. Cabibbo, W. Blum, E. Evangelista, M.E. Kassner, M.A. Meyers, Transmission electron microscopy study of strain induced low- and high-angle boundary development in equal-channel angular-pressed commercially pure aluminum, Metall. Mater. Trans. A39 (2008) 181-192.
[8] M. Cabibbo, A TEM Kikuchi pattern study of ECAP AA1200 via routes A, C, B_C, Mater. Character. 61 (2010) 613-625.
[9] C. Xu, Z. Horita, T.G. Langdon, The evolution of homogeneity in processing by high-pressure torsion, Acta Mater. 55 (2007) 203-212.
[10] G. Sakai, Z. Horita, T.G. Langdon, Grain refinement and superplasticity in an aluminum alloy processed by high-pressure torsion, Mater. Sci. Eng. A 393 (2005) 344-351.
[11] N.H. Polakowski, E.J. Ripling, Strength and Structure of Engineering Materials, Prentice-Hall, Englewood Cliffs, NJ, 1966.
[12] J. C. Russ, R., T. Dehoff, Practical Stereology, 2nd Ed. Springer Science & Business Media LLC New York, 2000.

[13] M. Cabibbo, P. Ricci, R. Cecchini, Z. Rymuza, J. Sullivan, S. Dub, S. Cohen, An international round-robin calibration protocol for nanoindentation measurements, Micron 43 (2012) 215-222.
[14] W.C. Oliver, G.M. Pharr, Measurement of hardness and elastic modulus by instrumented indentation: Advances in understanding and refinements to methodology, J. Mater. Res. 19 (2004) 3-20.
[15] N. Hansen, New discoveries in deformed metals, Metall. Mater. Trans. A 32 (2001) 2917-2935.
[16] T. Furu, R. Ørsund, E. Nes, Subgrain growth in heavily deformed aluminium—experimental investigation and modelling treatment, Acta Metall. 43 (1995) 2209–2232.
[17] R. Sandström, B. Lehtinen, E. Hedman, I. Groza, S. Karlsson, Subgrain growth in Al and Al-1% Mn during annealing, J. Mater. Sci. 13 (1978) 1229–1242.
[18] N. Hansen, X. Huang, G. Winther, Grain orientation, deformation microstructure and flow stress, Mater. Sci. Eng. A 494 (2008) 61-67.
[19] N. Hansen, Hall–Petch relation and boundary strengthening, Scripta Mater. 51 (2004) 801-806.
[20] N. Hansen, X. Huang, W. Pantleon, G. Winther, Grain orientation and dislocation patterns, Philos. Mag. 86 (2006) 3981-3994.
[21] W. Pantleon, N. Hansen, Disorientations in dislocation boundaries: formation and spatial correlation, Mater. Sci. Eng. A 309–310 (2001) 246-250.
[22] M.J. Starink, X.G. Qiao, J.W. Zhang, N. Gao, Predicting grain refinement by cold severe plastic deformation in alloys using volume averaged dislocation generation, Acta Mater. 57 (2009) 5796-5811.
[23] M. Cabibbo, S. Spigarelli, A TEM Quantitative Evaluation of Strengthening in an Mg-RE Alloy Reinforced with SiC, Mater. Character. 62 (2011) 959-969.
[24] J.W. Hutcchinson, Elastic-plastic behaviour of polycrystalline metals and composites. Proc. Roy. Soc. London Ser.A 319 (1970) 247-272.
[25] N. Hansen, X. Huang, Microstructure and flow stress of polycrystals and single crystals, Acta Mater. 46 (1998) 1827-1836.
[26] R. Neuhaus, Cb. Schwink, On the flow stress of [100]- and [111]-oriented Cu-Mn single crystals: A transmission electron microscopy study, Phil. Mag. 65 (1992) 1463-1484.
[27] J.W. Zhang, N. Gao, M.J. Starink, Microstructure development and hardening during high pressure torsion of commercially pure aluminium: Strain reversal experiments and a dislocation based model, Mater. Sci. Eng. A 528 (2011) 2581-2591.
[28] X.C. Qiao, M.J. Starink, N. Gao, Hardness inhomogeneity and local strengthening mechanisms of an Al1050 aluminium alloy after one pass of equal channel angular pressing, Mater. Sci. Eng. A 513 (2009) 52-58.
[29] E. Nes, T. Pettersen, K. Marthinsen, On the mechanisms of work hardening and flow-stress saturation, Scripa Mater. 43 (2000) 55-62.
[30] L.S. Tóth, Y. Estrin, R. Lapokov, C. Gu, A model of grain fragmentation based on lattice curvature, Acta Mater. 58 (2010) 1782-1794.
[31] J.R. Cahoon, W.H. Broughton, A.R. Kutzak, The determination of yield strength from hardness measurements, Mater. Trans. 2 (1971) 1979-1983.
[32] E. Broitman, Indentation Hardness Measurements at Macro-, Micro-, and Nanoscale: A Critical Overview, Tribol. Lett. 65 (2017) 23-41.
[33] M. Cabibbo, E. Santecchia, Microstructure and Intermetallic Strengthening in an Equal ChannelAngular Pressed AA2219. Part II: Strengthening Model, Metallogr. Microstruct. Anal. 3 (2014) 203-212.
[34] M. Cabibbo, C. Paoletti, B. Lasio, R. Orrù, F. Delogu, Indentation strain rate sensitivity ofball-milled spark-plasma sintered Cu-C metal matrix composite, J. All. Compd. 767 (2018) 838-847.

TABLE and FIGURE captions

Table 1. Equivalent strain, ε_{eq}, obtained by HPT N = 1/120, 1/72, and 1/45 turns, and r = 0.3, 0.6, 0.9, 0.12, and 0.15 mm from disc center. Bold values refer to the performed TEM inspections. The ε_{eq}^{1} = 0.05 is the minimum necessary strain to form cell boundaries from TD in 6N-Al.

Table 2. TD density, ρ_{TD}, measured at different strain levels, ε_{eq}, from ε_{eq} = 0.02 to 0.10.

Table 3. Proof stress, σ_y, and individual microstructure contributions (σ_{TD}, $\sigma_{VLAB+LAB}$, σ_{HAB}) as determined by Eq. (6a) and Eq. (6b).

Figure 1. TEM microstructure of the 6N-Al annealed at 655 K/60 min showing no dislocations within the coarse-grained structure, a); Scheme of the HPT disc of radius R and thickness t, b). The TEM disk sample extraction locations and distance, r, form disc centre are also shown.

Figure 2. Representative TEM micrographs of the 6N-Al subjected to SPD by HPT at N = 1/120, r = 0.3, ε_{eq} ~0.02, a), 0.6, ε_{eq} ~0.04, b), 0.9, ε_{eq} ~0.05, c), 1.2, ε_{eq} ~0.07, d), 1.5 mm, ε_{eq} ~0.09, 2e), at N = 1/72, r = 0.9, ε_{eq} ~0.09, f), at N = 1/45, r = 0.3, ε_{eq} ~0.05, 2g), and r = 0.6 mm, ε_{eq} ~0.10, h).

Figure 3. Representative TEM micrographs of the 6N-Al microstructure after ARB at ε_{eq} ~0.05, a), and ε_{eq} ~0.10, b).

Figure 4. Bright-Filed TEM showing a typical cell boundary from which the boundary dislocation spacing, S, was determined. Present case refers to ε_{eq} = 0.05 at HPT N = 1/45, r = 0.3 mm, where a very low-angle boundary (VLAB) showing Moiré fringes is shown. The method to measure dislocation spacing in boundaries showing Moiré fringes is reported elsewhere ([**6-8**] and references therein).

Figure 5. TEM micrograph of the 6N-Al at ε_{eq} = 0.24, obtained by HPT at N = 1/45 and r = 1.5 mm from the disc center. The microstructure shows the formation and presence of VLABs, LABs, and HABs, that contributed to constitute a fine-grained structure.

Figure 6. Representative nanoindentation load-displacement curves for samples strained by HPT at ε_{eq} = 0.02, 0.04, 0.05, 0.07, 0.09, and 0.10, a), and resulted hardness, $H_{nanoind}$, *vs.* strain, ε_{eq}, where the experimental error of ~20 MPa is within the data bars, b). In b) the $H_{nanoind}$ plot is compared to the H as estimated by the TEM inspections and strengthening model of Eqs. (6a) and (6b) and Table 3: $H_{nanoind}^{exp} = \sigma_y^{calc}/(2.9 \cdot 0.0945)$. The data referring to ε_{eq} = 0.24 are also reported.

Figure 7. Comparison among the nanoindentation hardness obtained at different dwelling times, t_{dwell} = 5-to-180 s compared to the hardness value derived from the strengthening model (Eq. (7)) in the HPT (N = 1/45, r = 1.5 mm) ε_{eq} = 0.24 condition.

Minimum necessary strain to induce tangled dislocation to form cell and grain boundaries in a 6N-Al

Marcello Cabibbo

DIISM / Università Politecnica delle Marche, Via Brecce Bianche 12, 60131 – Ancona, Italy.

Keywords: 6N-Aluminum; Dislocation structure; Cell structure; HPT; strengthening model; nanoindentation.

Abstract. Severe plastic deformation (SPD) techniques are known to promote exceptional material properties by inducing significant modifications in the metallic material microstructure. In particular, severe plastic deformation (SPD) techniques are known to effectively refine the initial grain structure of *f.c.c.* and *b.c.c.* crystals to sub-micrometre levels. Pure metals are mostly appropriate to study the early stages of the microstructure modifications induced by SPD. This is chiefly due to the possibility to isolate the material strengthening due to dislocations from other possible microstructure features. To this purpose, a high-purity 6N-aluminum (99.9999% purity) was here used to study the minimum necessary strain to form crystal boundaries (that is, cell and grain boundaries). Cell and grain boundaries are formed from previously introduced tangled dislocations (TD), which constitute the microstructure modification features at the early stages of plastic deformation. In this study, the 6N-Al was subjected to high-pressure torsion (HPT) by which the minimum necessary strain, ε_{eq}, to form cell boundaries was identified. It was thus find that, TD started to evolve to cell boundaries at ε_{eq} = 0.05. This finding was validated by a second SPD technique, such as accumulative roll bonding (ARB). A microstructure strengthening model was applied and validated by nanoindentation measurements.

1. Introduction

In the last few decades, thermally stable ultrafine-grained (UFG) metallic materials and alloys were widely studied and characterized as they showed superior mechanical properties compared to the conventional grained counterparts **[1]**. With this respect, a number of grain refining methods were proposed and developed so far. In particular, top-down approaches, such as severe plastic deformation (SPD) are the ones showing the most promising and technologically reliable techniques to obtain sound UFG metals **[2-4]**.

To understand the physical principles behind the SPD-driven UFG formation, pure metals are typically used. In particular, pure aluminum has a relatively low melting temperature (933 K) and a high stacking fault energy (γ_{SFE} = 166 mJ·m^{-2}). Pure Al, with different purity levels, was the referee metallic material used for a variety of fundamental studies involving all the most relevant SPD techniques. These include high-pressure torsion (HPT), equal-channel angular pressing (ECAP), accumulative roll-bonding (ARB), accumulative press-bonding (APB), twist extrusion (TE), friction stir processing (FSP), cyclic extrusion-compression (CEC), repetitive corrugation and straightening (RCS), accumulative back extrusion (ABE) and hydrostatic extrusion (HSE), high-pressure sliding (HPS) (**[4-6]** and references therein).

It is thus now widely recognized that the exceptional mechanical properties achieved by the UFG metals can be attributed to both the sub-micron cell, grain size and the mobile dislocations within grains. The evaluation of the tangled dislocations (TD) density is thus an important microstructure feature to understand the evolution from conventional-grained to UFG under SPD. Several published works **[4-10]** recognized that the UFG formation proceeds from TD and dense

dislocation walls (having very low-angle boundaries), which are continuously introduced in the material during SPD, and that eventually rearrange to form cell structures (low-angle boundaries, LABs). These latter are in turns induced to increase their misorientation angle to eventually become grain boundaries (high-angle boundaries, HABs). With this respect, the identification of the minimum necessary SPD strain to promote the newly introduced TD to form cell boundaries is an important issue for the UFG production processes.

The present study focused on the microstructure TEM-based determination of the minimum necessary strain to promote the formation of cell, and eventually grain boundaries, from tangled dislocations in a high-purity 99.9999% (6N-Al) aluminum. To this purpose, the 6N-Al was subjected to HPT, and eventually to ARB to double-check the results obtained by HPT.

HPT was used as it allows characterizing the early stages of shear plastic deformation induced in the material. In fact, HPT generates progressive plastic deformation levels from a minimum at the disc center, to a maximum at the disc periphery. The level of induced strain strongly depends on the number of HPT rotations, *N*. In HPT, the sample, in form of a thin disc, is placed between two large anvils and subjected to a high pressure and concurrent torsional straining. This way, the two meaningful parameters are the magnitude of the imposed pressure, *P*, and the number of revolutions applied to the sample, *N*. The imposed strain chiefly depends on the distance from the disc center, and thus the microstructure modifications imposed by HPT are greatly inhomogeneous by a continuous rate from disc periphery to its center. For the present study, this latter aspect is considered as a key microstructure aspect to determine the minimum necessary strain level to form cell boundaries by TD rearrangement. In this sense, HPT is different from most SPD processes, such ECAP, TE, or FSP, where strain gradients are generated quite quickly making almost impossible to determine the early stages of cell structure formation.

2. Experimental procedures and Method

2.1. The material

A 6N-Al (purity of 99.9999%) was used for this study. The 6N-Al was fully annealed at 655 K / 60 min. As shown in **Figure 1(a)**, the annealed aluminum showed a coarse-grained structure with quite few free dislocations within the grains. These few, short and dispersed free dislocations are likely to be generated as statistical phenomenon induced by annealing from the boundaries of the coarsening grains.

2.2. High-Pressure Torsion and Accumulative Roll Bonding methods

The annealed 6N-Al was subjected to HPT at different experimental conditions, to obtain an almost continuous range of strain levels, *i.e.*, from ε_{eq} = 0.02-to-0.24. **Figure 1(b)** is a schematic representation of the HPT strain deformation imposed to a typical disc sample. The incremental shear strain is given by $d\omega/\omega$, being ω the angular rotation around the disc center. The equivalent vön Mises strain imposed by HPT is calculated according to **[11]**, Eq. (1a):

$$\varepsilon = \frac{2}{\sqrt{3}} ln\left[\left(\frac{1+\gamma^2}{4}\right)^{0.5} + \frac{\gamma}{2}\right] \qquad \text{Eq. (1a)}$$

where $\gamma = (2\pi Nr)/t$ is the shear strain, *r* the distance from the disc center, ranging from 0 to *R* (disc radius), *t* the disc thickness. From Eq. (1a), the equivalent strain, ε_{eq}, variation with the distance to disc center is:

$$\varepsilon_{eq} = \frac{2\pi N r}{t\sqrt{3}}$$ Eq. (1b)

The initial disc radius, *R*, and thicknesses, *t*, were 20 mm and 1 mm, respectively. HPT was carried out at room-temperature by depressing the vertical anvils to a depth of 0.05 mm. Torsion strain was exerted by rotating the upper anvil at a low rotation speed of 0.17 rpm ($1°sec^{-1}$) under a pressure of 38 MPa (300 Kg load). In order to apply low rates of strain, the number of rotation were reduced to *N* = 1/120, 1/72, and 1/45. The disc flowed to the radial direction during HPT due to the lack of side constraint, resulting in a thickness reduction almost irrelevant, being, respectively, ~0.05, ~0.05, and ~0.06 mm, from the initial 1 mm disc thickness. TEM inspections were performed at the mid-section of the discs (that is, at a thickness $t \cong 0.5$ mm) at different distances from the disc center: ~0.3, ~0.6, ~0.9, ~1.2, and ~1.5 mm. The resulting equivalent strains, ε_{eq}, were calculated by Eq. (1b) and are listed in Table 1.

The reason to use HPT to perform the present study is based on the possibility to generate an almost continuous incremental strain level, starting form a minimum equivalent strain level as low as $\varepsilon_{eq} = 0.02$.

	distance to disc center, *r*, mm				
angular rotation, θ, °	~0.3	~0.6	~0.9	~1.2	~1.5
5 (*N*=1/120)	**0.02**	**0.04**	**0.05**[1]	**0.07**	**0.09**
10 (*N*=1/72)	0.03	0.06	**0.09**	0.12	0.15
15 (*N*=1/45)	**0.05**[1]	**0.10**	0.14	0.19	0.24

Table 1. Equivalent strain, ε_{eq}, obtained by HPT *N* = 1/120, 1/72, and 1/45 turns, and *r* = 0.3, 0.6, 0.9, 0.12, and 0.15 mm from disc center. Bold values refer to the performed TEM inspections. The $\varepsilon_{eq}{}^{1} = 0.05$ is the minimum necessary strain to form cell boundaries from TD in 6N-Al.

Yet, to double-check the soundness of the experimental results obtained by HPT, the annealed 6N-Al was also subjected to ARB at the same minimum strain level found by HPT to start forming cell/grain boundaries from TDs.

ARB was carried out on two equally-thick annealed 6N-Al strips to make a stacked thickness of 1 mm. These were roll bonded at room temperature to a 3% thickness reduction. A second round of ARB with same 3% thickness reduction was also performed. This way, the 6N-Al was subjected to a vön Misses equivalent strain of, respectively, ε_{eq} ~0.05, and ε_{eq} ~0.10. The rolls diameter were 80 mm and the roll peripheral speed was about 60 mm/min.

2.3. Sample preparation and Transmission electron Microscopy details

To avoid any possible artifact during sample preparation, the ~1 mm-thick HPT processed discs were prepared for TEM inspections by chemical and electro-chemical means only. They were punched to 3 mm TEM discs at HPT positions indicated in **Figure 1(b)**. The 3 mm-wide and ~1 mm-thick TEM discs were chemically thinned to ~200 μm using a solution of 15% HCl_4, 15% $C_3H_3(OH)_3$, 70% methanol. Finally, they were electro-chemically polished to electron transparency by double-jet with a solution of 1/3 nitric acid and 2/3 methanol at 238 K and V = 12V. TEM inspections were carried out using a Philips™ C-20® working at 200 keV with a double-tilt specimen holder equipped with a liquid-nitrogen cooling stage. Inspections were performed at the middle height of the HPT discs. Same procedures were followed to prepare the ARB TEM discs. In this latter case, discs were extracted along the ARB strip section and observations were carried out at the central zone of the two bonded strips.

Two-beam excitation conditions were selected for most of the TEM observation and dislocation characterizations. Tangled dislocation (TD) density, ρ_{TD}, was quantified using Ham's interception stereological methods [**12**]. Thence, ρ_{TD} was calculated through the count of interception points

between the mesh and the existing dislocations, n_{disl}, in the TEM micrographs. This was evaluated by $\rho_{TD} = 2n_{disl}/(l_{mesh}t_{TEM})$, were, l_{mesh} is the total length of the mesh, and t_{TEM} is the thickness of the TEM foil. Crystal thickness, t_{TEM}, was determined through the diffracted beam intensity variation under dual beam conditions, using converged electron beam diffraction (CBED) patterns. This way, by plotting the linear interpolation of data points in a $S^2/n_{fringes}^2$ vs. $n_{fringes}^{-2}$ graph, where S is the fringes spacing and $n_{fringes}$ the number of counted fringes, t_{TEM}^{-2} was determined at y-axis line intercept. The error due to the invisible dislocations (i.e., the ones oriented as to have $b \cdot g = 0$, where b is the Burgers vector and g refers to the dislocation lying crystallographic plane) is within the experimental error of the foil thickness evaluation. Cell (LAB) and grain boundary (HAB) misorientation were measured by Kikuchi band patterns. The misorientation angle measurement procedure by Kikuchi pattern on TEM is fully described elsewhere in previous published works by this author [**7,8**]. All TEM inspections were carried out by orienting the aluminum matrix [002] crystallographic plane parallel to the electron beam.

2.4. Nanoindentation methods

Nanoindentation measurements were performed at same HPT disc height as TEM inspections. For the nanoindentation measurements, samples were prepared by the same chemical thinning methods used for the TEM foil preparation. A Hysitron™ Triboscope UBI-1® was used. Calibration procedures were followed according to [**13**]. A trapezoidal load function of 5 s loading, 15 s at the set load, and 5s unloading was used, with a set load of 1000 μN. The reported data were averaged over a series of 4 8x8 matrix of individual measurements spaced 250 μm. Data analysis was performed according to the Oliver-Pharr method [**14**].

3. Experimental Results

The plastically deformed 6N-Al HPT microstructure at different HPT experimental conditions is reported in **Figure 2**. The Figure reports representative TEM micrographs taken at N = 1/120, r = 0.3 (Fig. 2a), 0.6 (Fig. 2b), 0.9 (Fig. 2c), 1.2 (Fig. 2d), 1.5 mm (Fig. 2e), at N = 1/72, r = 0.9 (Fig. 2f), at N = 1/45, r = 0.3 (Fig. 2g), and r = 0.6 mm (Fig. 2h). It appears that at the lowest strain levels ($\varepsilon_{eq} < 0.05$) the plastically deformed microstructure is only constituted by TDs, which have quite low dislocation density at $\varepsilon_{eq} = 0.02$ (Fig. 2a). These are induced to group with the strain. The ρ_{TD} values obtained at the different TEM inspected HPT conditions are listed in the Table 2. It resulted that, ρ_{TD} steadily increased from $\varepsilon_{eq} = 0.02$ to 0.05, to eventually slightly decrease at $\varepsilon_{eq} > 0.07$, in favour of the early formation of dislocation boundaries (*i.e.* cell boundaries). In fact, TEM inspections (Figs. 2e, f, h) clearly showed that at $\varepsilon_{eq} \cong 0.05$ cell boundaries started to form. At ε_{eq} = 0.09-0.10 some grain boundaries (HAB) were also detected (Fig. 2h). In particular, starting from the minimum necessary strain $\varepsilon_{eq} \cong 0.05$ to form dislocation boundaries, tangled dislocations (TDs) are continuously formed within the newly formed cell and grain structures. These can be seen also at the maximum strain level here inspected ($\varepsilon_{eq} \cong 0.10$ of Fig. 2h). This in turns means that the minimum necessary strain to induce the formation of cell, and eventually grain boundaries, can be identified as $\varepsilon_{eq} \cong 0.05$. That is, the initiation of microstructure refining process induced by the plastic deformation can be identified at a strain of $\varepsilon_{eq} \cong 0.05$. It is noteworthy that the dislocation densities here reported are quite low and this is likely to be due to the small strain applied to the 6N-aluminum.

The results obtained by HPT process were also verified by ARB. **Figure 3** shows representative TEM micrographs of the microstructure at ARB ε_{eq} ~0.05 (Fig. 3a) and ε_{eq} ~0.10 (Fig. 3b). It appeared that at ARB ε_{eq} ~0.05 no cell boundary formation were detected. This actually confirmed the soundness of the conclusions drawn by HPT. These experimental results seem to confirm that

ε_{eq} ~0.05 was the minimum necessary strain to form cell, and eventually grain boundaries in high-purity aluminum. This in turns mean that the UFG process starts to activate from a minimum strain level of ε_{eq} ~0.05 in SPD pure aluminum. The fine-grained structure formation is actually activated whenever a crystal region containing TDs is subjected to a sufficient strain gradient to induce ρ_{TD} rises as to eventually reach a critical (threshold) value. Above this threshold-like strain level, these dislocations start to commonly group to a certain crystallographic orientation, thus forming a cell wall (LAB). Under the effect of the shear deformation, LABs are induced to evolve into cell boundaries, and eventually to grain boundaries (HABs).

	ε_{eq}							
	0.02 *N*=1/120, *r* = 0.3 mm	0.04 *N*=1/120, *r* = 0.6 mm	0.05 *N*=1/120, *r* = 0.9 mm	0.05 *N*=1/45, *r* = 0.3 mm	0.07 *N*=1/120, *r* = 1.2 mm	0.09a *N*=1/120, *r* = 1.5 mm	0.09b *N*=1/72, *r* = 0.9 mm	0.10 *N*=1/45, *r* = 0.6 mm
ρ_{TD}, 10^{12} m^{-2}	3	18	235	180	160	55	86	62

Table 2. TD density, ρ_{TD}, measured at different strain levels, ε_{eq}, from ε_{eq} = 0.02 to 0.10.

4. Discussion

The here obtained microstructure results suggested a sort of correlation between the minimum necessary strain to initiate cell boundaries (LABs) formation and the amount of TDs that are generated during the plastic deformation. In fact, it was found that the TD density steadily increased with strain up to the strain level where cells and grains started to form. Starting from this strain level, the density of TDs, $\rho_{TD,}$ slightly reduced (Table 2). On one hand, this is chiefly due to a dislocation annihilation driven by dynamic recovery, due to the low melting temperature and high SFE of the 6N-Al. On the other hand, the $\rho_{TD,}$ reduction is due to the process of TD conversion to cell and grain boundaries, so to reduce the number density of dislocations within the cells and grains. These findings are in good agreement with other previously reported data [**15**].

The TD rearrangement, driven by the early stages of plastic deformation, is the microstructure process actually responsible for the grain refining process induced by both HPT and ARB. In fact, a large fraction of cell boundaries (LABs) evolving into grain boundaries (HABs) might migrate [**16**] or dissolve [**17**]. The cell boundary migration proceeds as collective movement of dislocation boundary perpendicular to the boundary plane. Cell boundary dissolution usually balance the number of cell boundary continuously formed from TDs. This in turns preserve the number fraction of the LABs during the early stages of UFG formation under SPD.

The fraction of TDs able to migrate are usually called geometrically necessary dislocations (GNDs) [**15,18,19**]. These accommodate strain gradients in non-homogeneous deformation proportionally to the strain gradient. GNDs are hard to annihilate since they statistically have the same sign associated with the direction of strain gradient. Another fraction of TDs is statistically stored by homogeneous deformation, and these are generally called statistically stored dislocations (SSDs) or incidental dislocations (IDs) [**18-20**]. They are likely to annihilate due to the balance of equal number of different sign dislocations randomly distributed within the crystal [**18**]. Thus, due to the high SFE of high-purity aluminum, microstructure evolution occurs by TD rearrangement at low levels and low deformation rates under HPT, as high strain levels are needed to achieve microstructural homogeneity. In particular, due to the specific strain path induced by HPT, the vast majority of dislocations, if not all of them, are GNDs [**17**].

Thus, the process of boundary formation from TDs can be described as follow. During shear plastic deformation, the newly formed TDs are induced to accumulate within the grains along specific crystallographic planes and directions. The preferential dislocation glide planes are the Al-[002] and the dislocations mostly accumulate along the Al-(200) directions. TDs tend to accumulate

to form series of broad linear zones characterized by long and highly dense dislocations. These, in turns, are induced to evolve into dense dislocation walls (DDWs). Whenever the DDWs are formed, the portion of the Al-matrix where they are located is locally deformed and a low misorientation of few tens to 1-1.5° is produced across the wall. This actually indicates that the new lines of DDWs generally represent discontinuities of the crystal uniformity within the aluminum grains. That is, the DDW structures consist of randomly oriented dislocation forming block of line defects that progressively rise their cumulative mean misorientation and get thinner with cumulative shear deformation.

Indeed, it was here shown that at a strain $\varepsilon_{eq} > 0.05$, the misorientation angles across the DDWs increased to a level by which DDWs assume the microstructure and mechanical character of cells, *i.e.* LABs (Fig. 3c). The width of DDWs gradually decrease and, correspondingly, the misorientation angles across DDWs increase progressively during straining. Thus, the formation of the DDWs, during straining, is likely to be due to a local accommodation process of the lattice curvatures at the zones of TD accumulation.

This argumentation is consistent with the analyses and models introduced by Hansen *et al.* [**20**]. In their model, they differentiate the TDs possibly forming low-misorientation dislocation lines, named as incidental dislocations (IDs), from the ones having larger misorientation, which are GNDs. These latter are considered the ones equivalent to the DDWs. It seems then that a dislocation substructure hierarchy governs the evolution of TDs to DDWs, occurring at the earlier stages of dislocation recombination to form cells (LABs) and grains (HABs). This process occurs above a specific local dislocation saturation limit. Thence, GNBs are the portion of free dislocations responsible for the formation of the cell and grain structure upon plastic deformation. In fact, at the site of the forest TDs forming DDWs, local lattice rotations is generated by excess dislocation density, which are always characterized by deformation-induced lattice rotations and long-range internal stresses. This microstructure evolution process indicates that the TD agglomerates that are induced by the plastic deformation are indeed dislocation walls (DWs) [**20**]. On the other hand, IDs are statistically formed free dislocation lines that move across the crystal under the effect of the external load. These are mobile line defects with minimal capability to form thick dislocation agglomerations. That is, from a statistical viewpoint IDBs do not contribute to form DDWs. On the contrary, GNDs are induced to accumulate and to form alternating misorientation angles depending on the different followed slip systems under external load [**21**].

Finally, the presence of grain boundaries, both the new and the ones formed on annealing can hinder the formation of wall-like structures. In fact, the grain boundary not only acts as an obstacle to dislocation motion, but also affects the resulting dislocation stress field. On the other hand, the crystallographic mismatch across a grain boundary is likely to accelerate the emission away or absorption into the boundary line of dislocations. In the present case, the initial 6N-Al annealing state consisted of quite wide grained-structure with grain size higher than 100 μm. Thus, the resulting wide grain boundary network had a limited hindering effect on the generation of TDs and eventual formation of DDWs during the early stages of plastic deformation.

To verify the soundness of the results obtained by the TEM microstructure inspections, a strengthening model was also applied. This model included all the meaningful microstructure features. Thus, the 6N-Al yield stress, σ_y, was determined both by linearly adding the microstructure terms, and by hardness measurements by nanoindentation. The microstructure strengthening model was determined as, Eq. (2a):

$$\sigma_y = \sigma_0 + \sigma_{Dislocations} = \sigma_0 + \sigma_{TD} + (\sigma_{VLAB} + \sigma_{LAB} + \sigma_{GB}) \qquad \text{Eq. (2a)}$$

where σ_0 = 10 MPa is the frictional stress of pure Al [**7**], σ_{TD} the stress due to the TDs, σ_{VLAB} the contribution form the cell boundaries with misorientation angle within 2° (very-low angle boundaries, VLABs), σ_{LAB} and σ_{GAB} the contribution coming from the cell (LAB) and grain (HAB) boundaries, respectively. This strengthening model was first introduced by Hansen and the Risø

group accounting for contributions coming from TDs, LABs, and HABs [**19**]. A more recent strengthening model, reported by the present author in [**7**], also included the strengthening contribution coming from VLAB (θ_{mis} <2°). According to the TEM observations, for strain levels ε_{eq} < 0.05, the yield stress is expected to be limited to, Eq. (2b):

$$\sigma_y|_{\varepsilon<0.05} = \sigma_0 + \sigma_{TD} \quad \text{Eq.(2b)}$$

On the other hand, at ε_{eq} = 0.05-0.15, Eq. (2) can be rewritten as, Eq. (2c):

$$\sigma_y(\varepsilon=0.05\text{-}0.15) = \sigma_0 + \sigma_{TD} + (\sigma_{VLAB} + \sigma_{LAB}) \quad \text{Eq.(2c)}$$

According to [**22,23**], being the TDs essentially coincident with the GNDs ($\rho_{TD} \cong \rho_{GND}$), σ_{TD} can be calculated as, Eq. (3):

$$\sigma_{TD} = M\alpha Gb\rho_{TD}^{0.5} \quad \text{Eq.(3)}$$

where M = 2.94 is the Taylor factor [**24,25**], α is a fitting constant ranging 0.2-0.3, and usually agreed to be 0.24 [**6,18,25,26**], G = 26 GPa is the shear modulus of aluminum, and b = 0.286 is the aluminum Burgers vector.

Since at low strain levels, *i.e.* ε_{eq} < 0.10 the detected volume fraction of the cell boundaries was quite low, and that of the grain boundaries was even lower, the strengthening contribution of these could be estimated by taking into account the mean dislocation density forming those boundaries. Thus, according to Hansen *et al.* [**18],** the following relationships were taken into account, Eq. (4a):

$$\sigma_{VLAB} + \sigma_{LAB} = \sigma_{VLAB+LAB} = M\alpha Gb\rho_{VLAB+LAB}^{0.5} \quad \text{Eq.(4a)}$$

where $\rho_{VLAB+LAB}$ is the average dislocation density that form the very-low angle and low-angle boundaries. These are here considered together, since in the early stages of cell boundary formation from TDs, the misorientation angle was found to be within 8°, with a large fraction of boundary misorientation ranging 2-to-6°.

Anyway, the approach of Eq. (4a) typically holds for a network of boundaries typical of refined or mixed cell/grained microstructures. In the present case, for strains 0.05 < ε_{eq} < 0.10, the volume fraction of cell boundaries, and even grain boundaries, was found to be quite low. That is, the newly formed boundaries are rather scattered in the 6N-Al microstructure. These boundaries have mostly low misorientation angles with few dislocations forming the boundary lines. Thus, to evaluate the cell boundary contribution the approach proposed by Starink and co-workers [**22,27,28]** was here taken into account, Eq. (4b):

$$\sigma_{VLAB+LAB} = (\alpha' GbS/4.365)\rho_{VLAB+LAB} \quad \text{Eq.(4b)}$$

where α' = 2 [**28,29**], S is the average distance between the boundary dislocations. This relationship holds for the LABs strengthening contribution.

According to [**27,30**], the strengthening contribution given by the few grain boundaries that were formed at 0.07 <ε_{eq} < 0.10, was modelled as, Eq. (5):

$$\sigma_{HAB} = \left(\frac{\alpha' Gb}{4.365}\right)\frac{b\rho_{HAB}}{arctg(b/S)} \quad \text{Eq.(5)}$$

Thus, Eq. (2b) and Eq. (2c) become Eq. (6a) and Eq. (6b), respectively:

$$\sigma_y|_{\varepsilon<0.05} = \sigma_0 + M\alpha Gb\rho_{TD}^{0.5} \quad \text{Eq.(6a)}$$

$$\sigma_y|_{\varepsilon>0.05} = \sigma_0 + M\alpha Gb\rho_{TD}^{0.5} + (\alpha' GbS/4.365)\rho_{VLAB+LAB} + \left(\frac{\alpha' Gb}{4.365}\right)\frac{b\rho_{HAB}}{arctg(b/S)} \quad \text{Eq.(6b)}$$

The average distance S of, respectively, LAB, Eq. (4b), and HAB, Eq. (5), was evaluated by TEM inspections. **Figure 4** shows a representative TEM micrograph from which these measurements were carried out.

Table 3 reports the 6N-Al yield stress as determined by the Eq. (6a) and Eq. (6b) for the lower strain levels, *i.e.* $\varepsilon_{eq} < 0.10$.

	ε_{eq}							
	0.02 *N*=1/120, *r* = 0.3 mm	0.04 *N*=1/120, *r* = 0.6 mm	0.05 *N*=1/120, *r* = 0.9 mm	0.05 *N*=1/45, *r* = 0.3 mm	0.07 *N*=1/120, *r* = 1.2 mm	0.09a *N*=1/120, *r* = 1.5 mm	0.09b *N*=1/72, *r* = 0.9 mm	0.10 *N*=1/45, *r* = 0.6 mm
σ_{TD}, MPa	9	22	26	22	21	13	17	15
$\sigma_{VLAB+LAB}$, MPa	-	-	6	5	9	11	8	14
σ_{HAB}, MPa	-	-	-	-	-	4	5	11
σ_y, MPa	**19**	**32**	**42**	**37**	**40**	**38**	**40**	**50**

Table 3. Proof stress, σ_y, and individual microstructure contributions (σ_{TD}, $\sigma_{VLAB+LAB}$, σ_{HAB}) as determined by Eq. (6a) and Eq. (6b).

From strain levels $\varepsilon_{eq} > 0.15$, as the strain rises, the cell and grain boundaries increased steadily. Thus, the aluminum microstructure develops a significant volume fraction of cell and grain boundaries. In particular, for a strain level $\varepsilon_{eq} > 0.20$, the microstructure can be already considered as a fine-grained structure characterized by both cell and grain boundary networks. Thence, for these strain levels, the following strengthening model is likely to be the appropriate approach, Eq. (7) [**6,7**]:

$$\sigma_y|_{\varepsilon>0.20} = \sigma_0 + M\alpha Gb\rho_{TD}^{0.5} + M\alpha G[(3b\theta_{LAB}((1-f_{HAB})/d_{LAB}))^{0.5} + k_{HP}(f_{HAB}/d_{HAB})^{0.5}] \quad \text{Eq.(7)}$$

Figure 5 shows the fine-grained microstructure of the 6N-Al as obtained by the maximum strain level of $\varepsilon_{eq} = 0.24$ obtained by HPT (N = 1/45, r = 1.5 mm). The microstructure appeared composed by TDs, cells and grains. This is indeed a typical sub-micrometre microstructure generated by HPT or similar SPD techniques. The 6N-Al yield stress obtained for $\varepsilon_{eq} = 0.24$ by Eq. (7) was σ_y = (105 ± 15) MPa. In fact, at this strain level, the fraction of HAB was less than 0.15%, with mean cell size d_{LAB} = 2.8 μm and mean misorientation θ_{LAB} = 7°. Thus, the contribution given by the TD was σ_{TD} = 38 MPa, the one given by the cells was $\sigma_{LAB} \cong$ 62 MPa, and the one given by the few grains was $\sigma_{HAB} \cong$ 5 MPa.

This TEM-based microstructure approach was verified by mechanical tests, using nanoindentation measurements. To this purpose, the applied load was the minimum possible according to the specific calibration procedure here followed (see [**13**], for further details). Indentation load was thus P = 1000 μN, since even lower loads would generate a significant scatter of hardness data that would have jeopardize the readability of the obtained results. By applying a load P = 1000 μN a mean experimental error of ~10% was obtained. **Figure 6(a**) shows

nanoindentation load-displacement curves for ε_{eq} = 0.02-to-0.10, referring to the HPT experimental conditions highlighted in bold numbers in Table 1 (the ones experimentally inspected by TEM).

A linear relationship holds between hardness, H_V, and yield stress, given by $H_V = (\sigma_y/3)\cdot(0.1)^{m-2}$, where m is the Meyer's hardness coefficient [**31**]. In the aluminum cold-rolled and annealed metallurgical status, this relationship reduces to $H_V = \sigma_V/\chi$, where χ =2.9-2.8 [**6**,**30**-**33**]. Moreover, the nanoindentation hardness ($H_{nanoind}$) can be converted into H_V by a factor of 0.0945, that is $H_V = 0.0945\cdot H_{nanoind}$ [**32**]. Thus, to correlate the results obtained by the microstructure model of Eqs. (6a) and (6b), two curves were plotted in **Figure 6(b)**. A first curve refers to the measured nanoindentation hardness $H_{nanoind}$; a second curve refers to the quantity $\sigma_y/(2.9\cdot0.0945)$ both plotted as a function of the strain level, ε_{eq}. The quantity $\sigma_y/(2.9\cdot0.0945)$ represents the expected hardness measured by nanoindentation $H_{nanoind}^{exp}$, where σ_y is determined by the TEM microstructure analyses and the applied strengthening model.

It resulted that the measured, $H_{nanoind}$, and the calculated, $H_{nanoind}^{exp}$, hardness trends with equivalent strain were quite similar, this latter appearing constantly below the $H_{nanoind}$ curve. That is, the nanoindentation measurements were able to confirm the soundness of the microstructure-based approach here reported. In fact, the measured hardness, $H_{nanoind}$, essentially followed the same trend of the $H_{nanoind}^{exp}$ that was obtained by the microstructure-based model. On the other hand, the hardness overestimation by the nanoindentation direct measurements is likely to be due to a local hardening effect of the Berkovich tip. Even if the applied load was quite low (P = 1 mN), a small offset of the hardness reading can be generated. This is most likely due to a certain amount of aluminum hardening generated by holding the tip in contact to the soft material during the measurements. The tip contact holding time was fixed at 15 s, and lower times would have made the loading curves virtually non-reliable, due to the large amount of instrumental transducer noise. As a matter of fact, also the nanoindentation hardness measurement of the ε_{eq} = 0.24 (HPT, N = 1/45, r = 1.5 mm) experimental condition showed values slightly higher than the ones obtained by converting the obtained yield stress to equivalent hardness, $H_{nanoind}^{exp}$ (ε_{eq} = 0.24) (**Fig. 6(b)**).

The occurrence of 6N-Al hardening under Berkovich tip contact was verified by tuning the dwelling time of the trapezoid load function. That is, a series of indentation at different dwelling times, t_{dwell} = 5, 10, 15, 20, 30, 60, 90, 120, 180 s, and same load-unload rates of 1 mN/5s were carried out in the sample at ε_{eq} = 0.24 (HPT, N = 1/45, r = 1.5 mm) condition. To this purpose, 5 different measurements were performed at each of the set t_{dwell}. **Figure 7** reports the mean hardness obtained over the 5 individual measurements at the different set t_{dwell}. It appeared that, for t_{dwell} = 5 and 10 s the hardness values are rather scattered and fuzzy, jeopardizing the actual evaluation of the data. At t_{dwell} = 15 and 20 s, the discrepancy between the measured values and the ones calculated by the strengthening model is of ~20 MPa. For dwelling times 20 < t_{dwell} < 90 s, the discrepancy tended to saturate to the amount obtained already at t_{dwell} = 15 and 20 s. For $t_{dwell} \geq$ 90 s, the measured hardness started to further deviate from the calculated value. As already reported by Cabibbo *et al.* in [**34**], and as expected by the references therein, this further deviation is due to a room-temperature creep phenomenon to which aluminum is subjected under constant tip load. Thence, the data reported in **Figure 7** well explain that the overestimation of the hardness by nanoindentation, compared to the hardness values obtained by the microstructure-based model, is likely to be attributed to a tip load material hardening mechanism.

5. Conclusions

In this study, the early stages of plastic deformation in high-purity 6N-aluminum were investigated by high-pressure torsion (HPT) technique. HPT allowed to characterize the microstructure modification and evolution for quite low strain levels, ε_{eq} = 0.02-to-0.24. HPT

results were validated by a SPD ARB technique. A strengthening model also validated the microstructure findings.
The following conclusions can be outlined.

a. A minimum necessary strain level to promote the boundary formation (low-angle boundaries) starting from tangled dislocations was determined as $\varepsilon_{eq} \sim 0.05$.
b. A strengthening model was applied to identify the microstructure features contributing to the aluminum strengthening induced by the early stages of plastic deformation.
c. To validate the soundness of the obtained results by TEM inspections and the related strengthening model, nanoindentation measurements were carried out at the lowest possible load of 1000 μN were performed. Experimental data followed quite closely the calculated hardness obtained applying the strengthening model. In particular, the nanoindentation hardness values were constantly higher than the values derived from the strengthening model.
d. The nanoindentation data overestimation was found to be most likely due to a tip load hardening effect occurring during the nanoindentation tests.

Acknowledgements: The author is grateful to "Istituto Sperimentale Metalli Leggeri" of Novara for the 6N-Al material delivery. Mr. M. Pieralisi is acknowledged for the HPT tests.

References

[1] X.X. Huang, N. Hansen, N. Tsuji, Hardening by annealing and softening by deformation in nanostructured metals, Science 312 (2006) 249-251.
[2] I.A. Ovid'ko, R.Z. Valiev, Y.T. Zhu, Review on superior strength and enhanced ductility of metallic nanomaterials, Prog. Mater. Sci. 94 (2018) 462-540.
[3] M. Cabibbo, Nanostructured Cobalt Obtained by Combining Bottom-Up and Top-Down Approach, Metals 8(11) (2018) 962-971.
[4] I. Sabirova, M.Yu. Murashkin, R.Z. Valiev, Nanostructured aluminium alloys produced by severe plastic deformation: New horizons in development Mater. Sci. Eng. A 560 (2013) 1-24.
[5] Y. Ito, K. Edalati, Z. Horita, High-pressure torsion of aluminum with ultrahigh purity (99.9999%) and occurrence of inverse Hall-Petch relationship, Mater. Sci. Eng. A 679 (2017) 428-434.
[6] M. Cabibbo, Microstructure strengthening mechanisms in different equal channel angular pressed aluminum alloys, Mater. Sci. Eng. A560 (2013) 413-432.
[7] M. Cabibbo, W. Blum, E. Evangelista, M.E. Kassner, M.A. Meyers, Transmission electron microscopy study of strain induced low- and high-angle boundary development in equal-channel angular-pressed commercially pure aluminum, Metall. Mater. Trans. A39 (2008) 181-192.
[8] M. Cabibbo, A TEM Kikuchi pattern study of ECAP AA1200 via routes A, C, B_C, Mater. Character. 61 (2010) 613-625.
[9] C. Xu, Z. Horita, T.G. Langdon, The evolution of homogeneity in processing by high-pressure torsion, Acta Mater. 55 (2007) 203-212.
[10] G. Sakai, Z. Horita, T.G. Langdon, Grain refinement and superplasticity in an aluminum alloy processed by high-pressure torsion, Mater. Sci. Eng. A 393 (2005) 344-351.
[11] N.H. Polakowski, E.J. Ripling, Strength and Structure of Engineering Materials, Prentice-Hall, Englewood Cliffs, NJ, 1966.
[12] J. C. Russ, R., T. Dehoff, Practical Stereology, 2nd Ed. Springer Science & Business Media LLC New York, 2000.

[13] M. Cabibbo, P. Ricci, R. Cecchini, Z. Rymuza, J. Sullivan, S. Dub, S. Cohen, An international round-robin calibration protocol for nanoindentation measurements, Micron 43 (2012) 215-222.
[14] W.C. Oliver, G.M. Pharr, Measurement of hardness and elastic modulus by instrumented indentation: Advances in understanding and refinements to methodology, J. Mater. Res. 19 (2004) 3-20.
[15] N. Hansen, New discoveries in deformed metals, Metall. Mater. Trans. A 32 (2001) 2917-2935.
[16] T. Furu, R. Ørsund, E. Nes, Subgrain growth in heavily deformed aluminium—experimental investigation and modelling treatment, Acta Metall. 43 (1995) 2209–2232.
[17] R. Sandström, B. Lehtinen, E. Hedman, I. Groza, S. Karlsson, Subgrain growth in Al and Al-1% Mn during annealing, J. Mater. Sci. 13 (1978) 1229–1242.
[18] N. Hansen, X. Huang, G. Winther, Grain orientation, deformation microstructure and flow stress, Mater. Sci. Eng. A 494 (2008) 61-67.
[19] N. Hansen, Hall–Petch relation and boundary strengthening, Scripta Mater. 51 (2004) 801-806.
[20] N. Hansen, X. Huang, W. Pantleon, G. Winther, Grain orientation and dislocation patterns, Philos. Mag. 86 (2006) 3981-3994.
[21] W. Pantleon, N. Hansen, Disorientations in dislocation boundaries: formation and spatial correlation, Mater. Sci. Eng. A 309–310 (2001) 246-250.
[22] M.J. Starink, X.G. Qiao, J.W. Zhang, N. Gao, Predicting grain refinement by cold severe plastic deformation in alloys using volume averaged dislocation generation, Acta Mater. 57 (2009) 5796-5811.
[23] M. Cabibbo, S. Spigarelli, A TEM Quantitative Evaluation of Strengthening in an Mg-RE Alloy Reinforced with SiC, Mater. Character. 62 (2011) 959-969.
[24] J.W. Hutcchinson, Elastic-plastic behaviour of polycrystalline metals and composites. Proc. Roy. Soc. London Ser.A 319 (1970) 247-272.
[25] N. Hansen, X. Huang, Microstructure and flow stress of polycrystals and single crystals, Acta Mater. 46 (1998) 1827-1836.
[26] R. Neuhaus, Cb. Schwink, On the flow stress of [100]- and [111]-oriented Cu-Mn single crystals: A transmission electron microscopy study, Phil. Mag. 65 (1992) 1463-1484.
[27] J.W. Zhang, N. Gao, M.J. Starink, Microstructure development and hardening during high pressure torsion of commercially pure aluminium: Strain reversal experiments and a dislocation based model, Mater. Sci. Eng. A 528 (2011) 2581-2591.
[28] X.C. Qiao, M.J. Starink, N. Gao, Hardness inhomogeneity and local strengthening mechanisms of an Al1050 aluminium alloy after one pass of equal channel angular pressing, Mater. Sci. Eng. A 513 (2009) 52-58.
[29] E. Nes, T. Pettersen, K. Marthinsen, On the mechanisms of work hardening and flow-stress saturation, Scripa Mater. 43 (2000) 55-62.
[30] L.S. Tóth, Y. Estrin, R. Lapokov, C. Gu, A model of grain fragmentation based on lattice curvature, Acta Mater. 58 (2010) 1782-1794.
[31] J.R. Cahoon, W.H. Broughton, A.R. Kutzak, The determination of yield strength from hardness measurements, Mater. Trans. 2 (1971) 1979-1983.
[32] E. Broitman, Indentation Hardness Measurements at Macro-, Micro-, and Nanoscale: A Critical Overview, Tribol. Lett. 65 (2017) 23-41.
[33] M. Cabibbo, E. Santecchia, Microstructure and Intermetallic Strengthening in an Equal ChannelAngular Pressed AA2219. Part II: Strengthening Model, Metallogr. Microstruct. Anal. 3 (2014) 203-212.
[34] M. Cabibbo, C. Paoletti, B. Lasio, R. Orrù, F. Delogu, Indentation strain rate sensitivity ofball-milled spark-plasma sintered Cu-C metal matrix composite, J. All. Compd. 767 (2018) 838-847.

TABLE and FIGURE captions

Table 1. Equivalent strain, ε_{eq}, obtained by HPT N = 1/120, 1/72, and 1/45 turns, and r = 0.3, 0.6, 0.9, 0.12, and 0.15 mm from disc center. Bold values refer to the performed TEM inspections. The ε_{eq}^{1} = 0.05 is the minimum necessary strain to form cell boundaries from TD in 6N-Al.

Table 2. TD density, ρ_{TD}, measured at different strain levels, ε_{eq}, from ε_{eq} = 0.02 to 0.10.

Table 3. Proof stress, σ_y, and individual microstructure contributions (σ_{TD}, $\sigma_{VLAB+LAB}$, σ_{HAB}) as determined by Eq. (6a) and Eq. (6b).

Figure 1. TEM microstructure of the 6N-Al annealed at 655 K/60 min showing no dislocations within the coarse-grained structure, a); Scheme of the HPT disc of radius R and thickness t, b). The TEM disk sample extraction locations and distance, r, form disc centre are also shown.

Figure 2. Representative TEM micrographs of the 6N-Al subjected to SPD by HPT at N = 1/120, r = 0.3, ε_{eq} ~0.02, a), 0.6, ε_{eq} ~0.04, b), 0.9, ε_{eq} ~0.05, c), 1.2, ε_{eq} ~0.07, d), 1.5 mm, ε_{eq} ~0.09, 2e), at N = 1/72, r = 0.9, ε_{eq} ~0.09, f), at N = 1/45, r = 0.3, ε_{eq} ~0.05, 2g), and r = 0.6 mm, ε_{eq} ~0.10, h).

Figure 3. Representative TEM micrographs of the 6N-Al microstructure after ARB at ε_{eq} ~0.05, a), and ε_{eq} ~0.10, b).

Figure 4. Bright-Filed TEM showing a typical cell boundary from which the boundary dislocation spacing, S, was determined. Present case refers to ε_{eq} = 0.05 at HPT N = 1/45, r = 0.3 mm, where a very low-angle boundary (VLAB) showing Moiré fringes is shown. The method to measure dislocation spacing in boundaries showing Moiré fringes is reported elsewhere ([**6-8**] and references therein).

Figure 5. TEM micrograph of the 6N-Al at ε_{eq} = 0.24, obtained by HPT at N = 1/45 and r = 1.5 mm from the disc center. The microstructure shows the formation and presence of VLABs, LABs, and HABs, that contributed to constitute a fine-grained structure.

Figure 6. Representative nanoindentation load-displacement curves for samples strained by HPT at ε_{eq} = 0.02, 0.04, 0.05, 0.07, 0.09, and 0.10, a), and resulted hardness, $H_{nanoind}$, *vs.* strain, ε_{eq}, where the experimental error of ~20 MPa is within the data bars, b). In b) the $H_{nanoind}$ plot is compared to the H as estimated by the TEM inspections and strengthening model of Eqs. (6a) and (6b) and Table 3: $H_{nanoind}^{exp} = \sigma_y^{calc}/(2.9 \cdot 0.0945)$. The data referring to ε_{eq} = 0.24 are also reported.

Figure 7. Comparison among the nanoindentation hardness obtained at different dwelling times, t_{dwell} = 5-to-180 s compared to the hardness value derived from the strengthening model (Eq. (7)) in the HPT (N = 1/45, r = 1.5 mm) ε_{eq} = 0.24 condition.

Figure 1a

Click here to download high resolution image

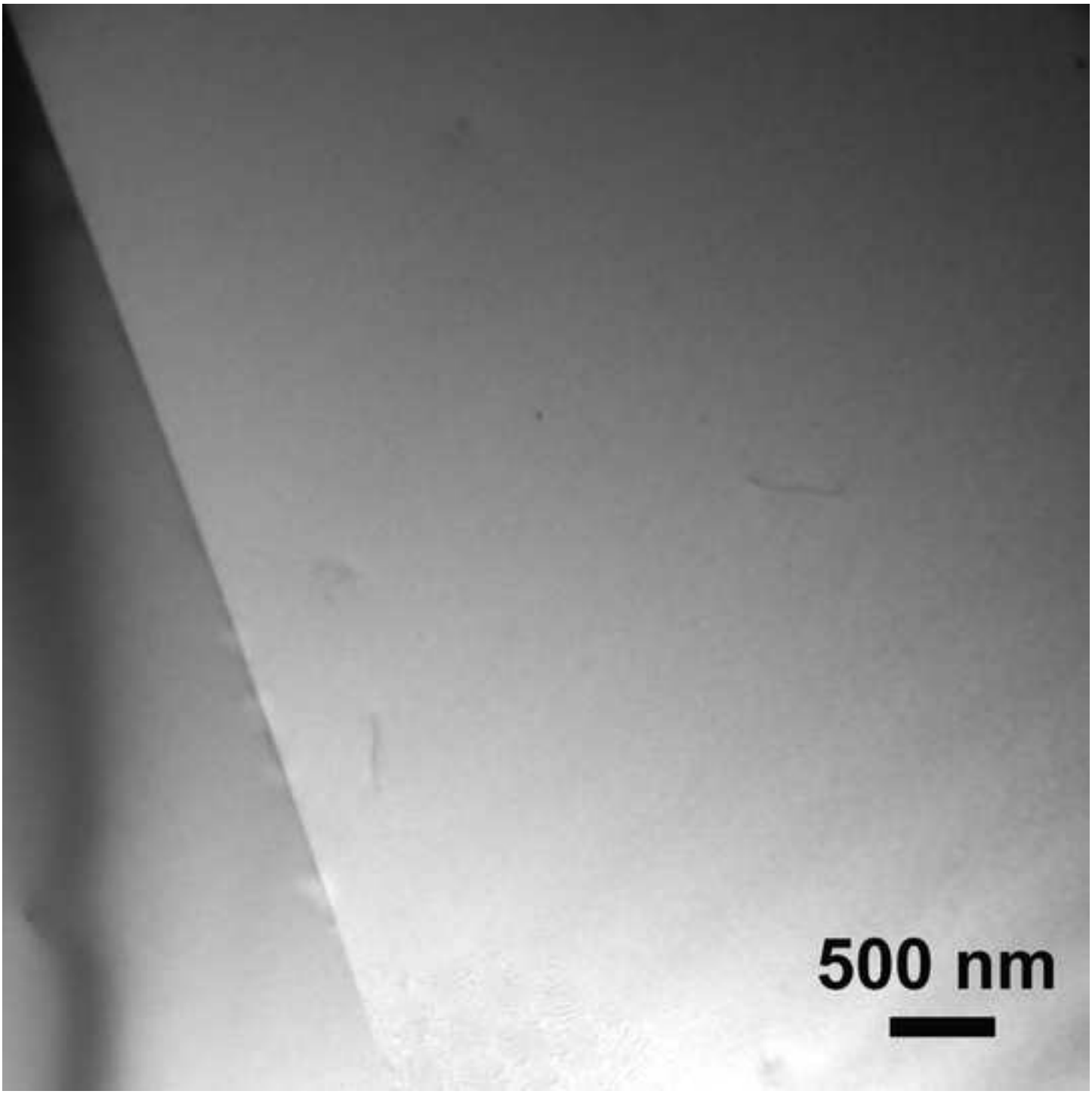

Figure 1b

Click here to download high resolution image

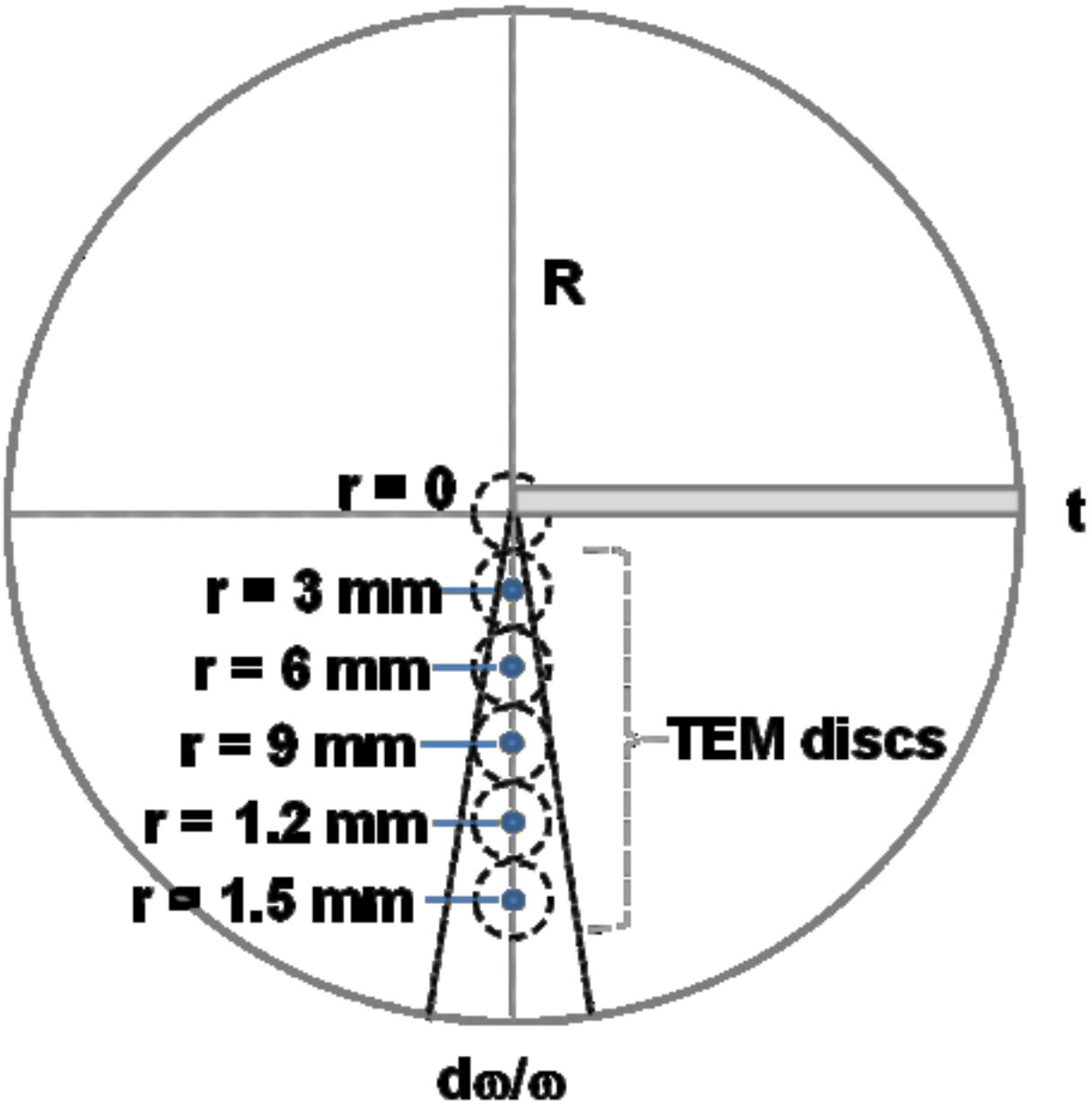

Figure 2a

Click here to download high resolution image

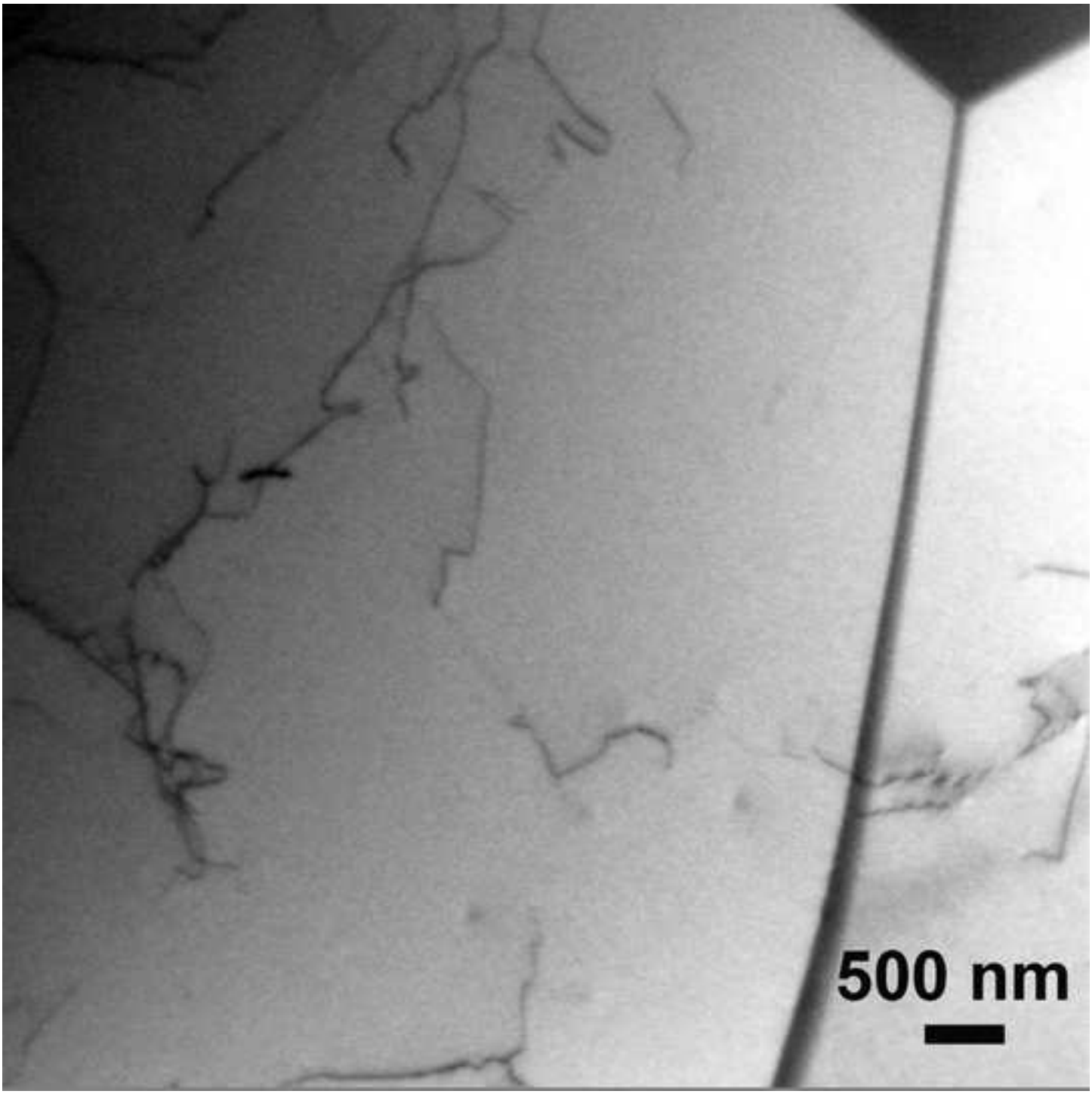

Figure 2b

Click here to download high resolution image

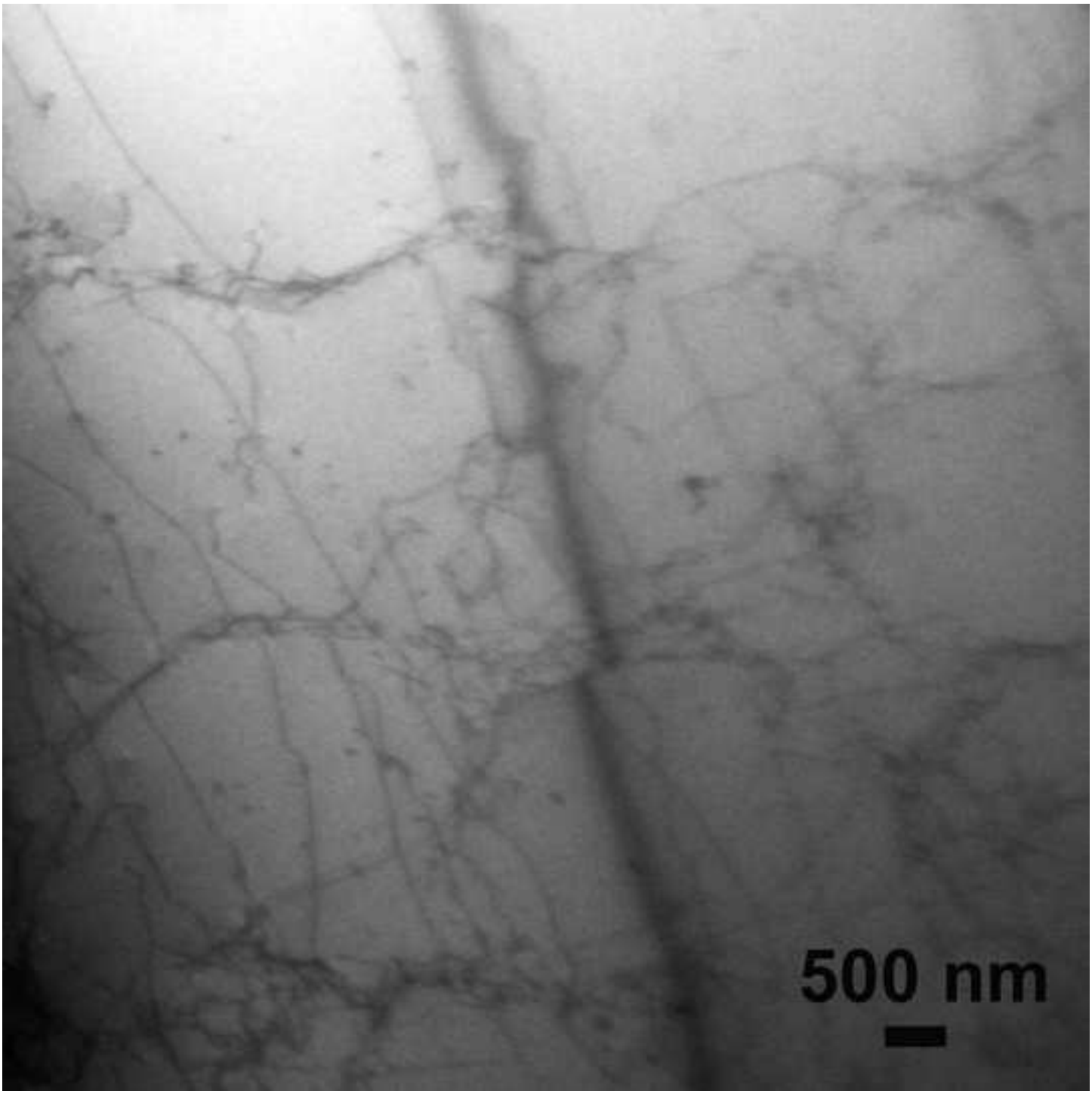

Figure 2c

Click here to download high resolution image

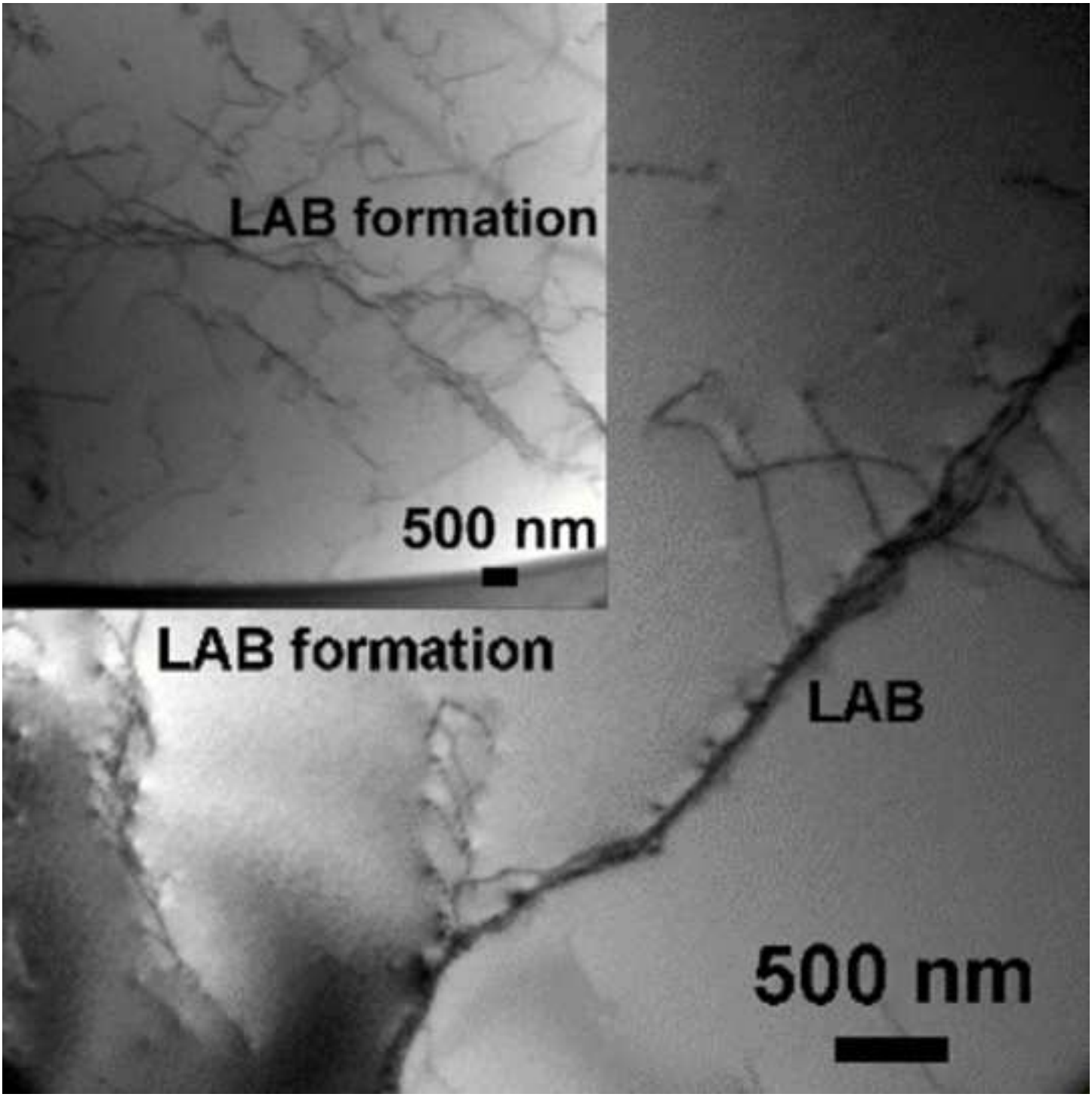

Figure 2d

Click here to download high resolution image

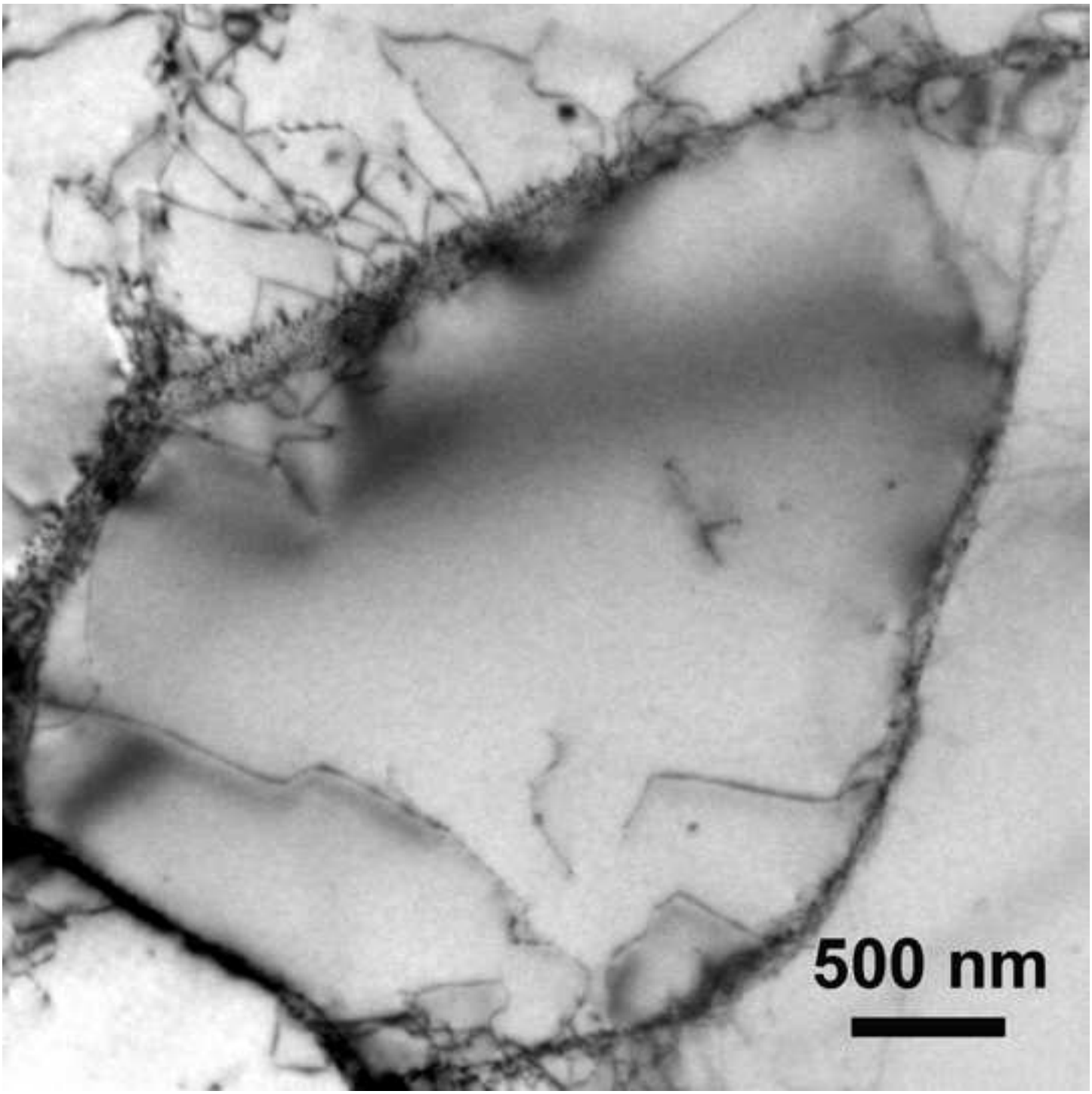

Figure 2e

Click here to download high resolution image

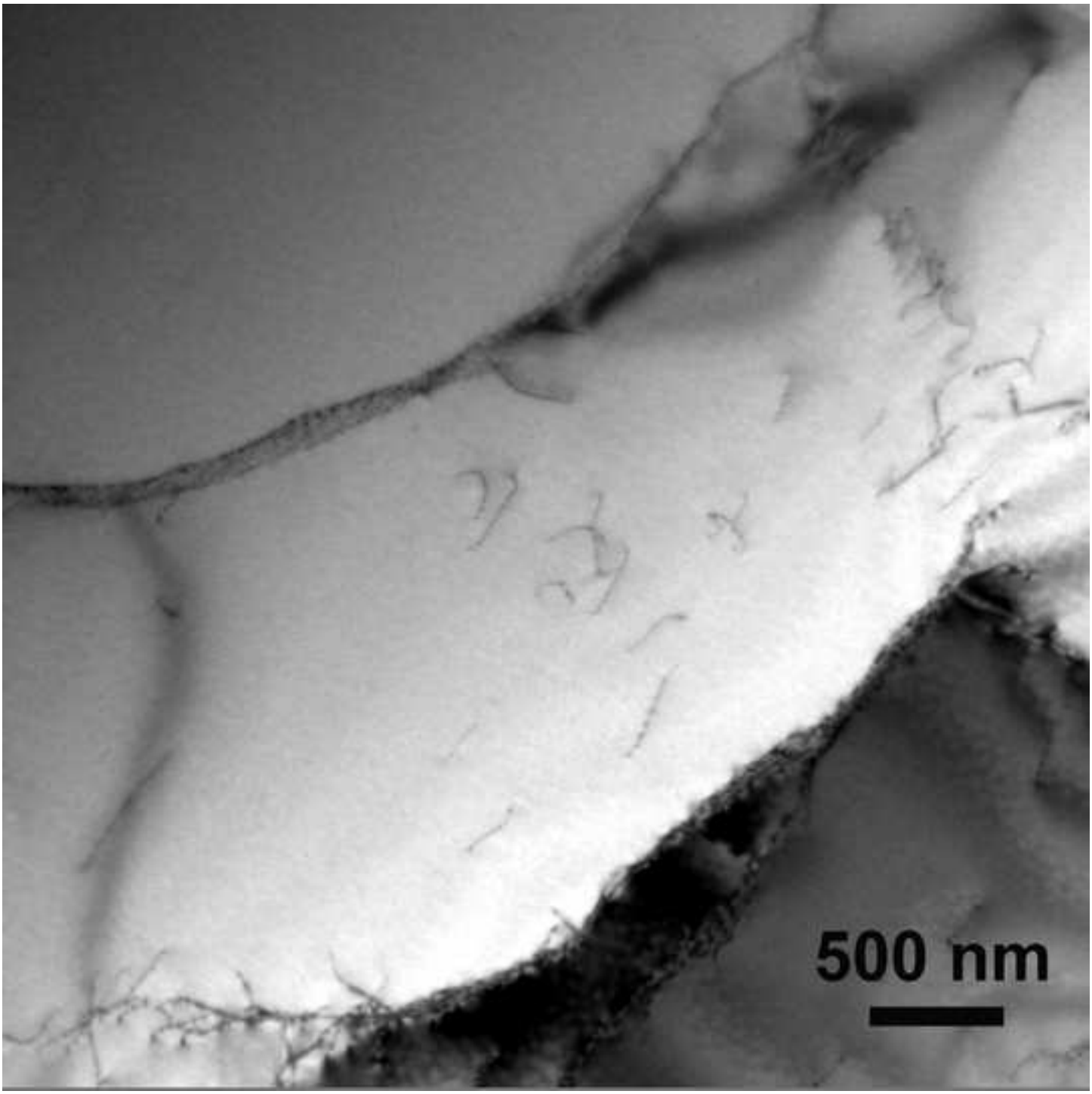

Figure 2f

Click here to download high resolution image

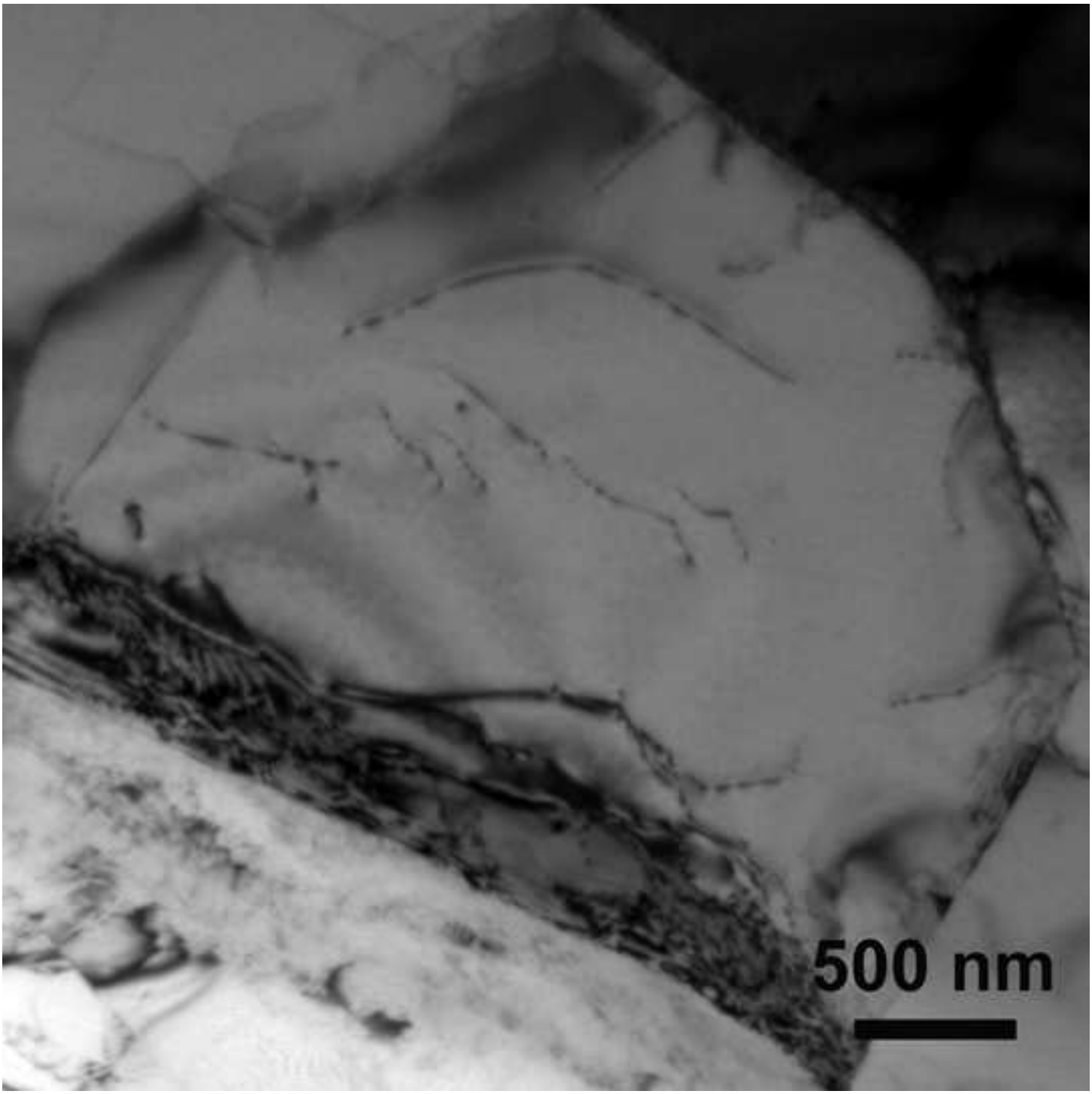

Figure 2g

Click here to download high resolution image

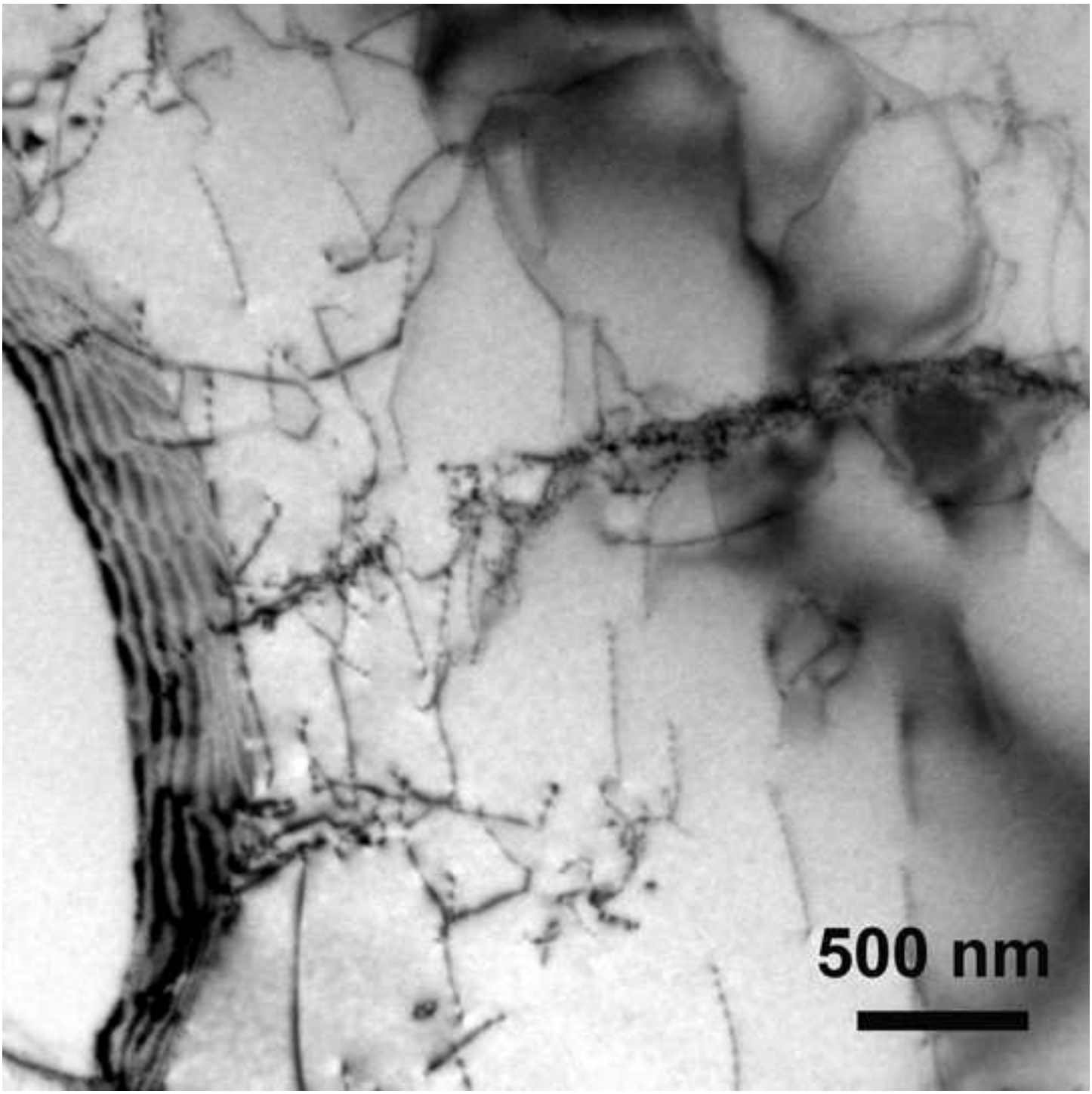

Figure 2h

Click here to download high resolution image

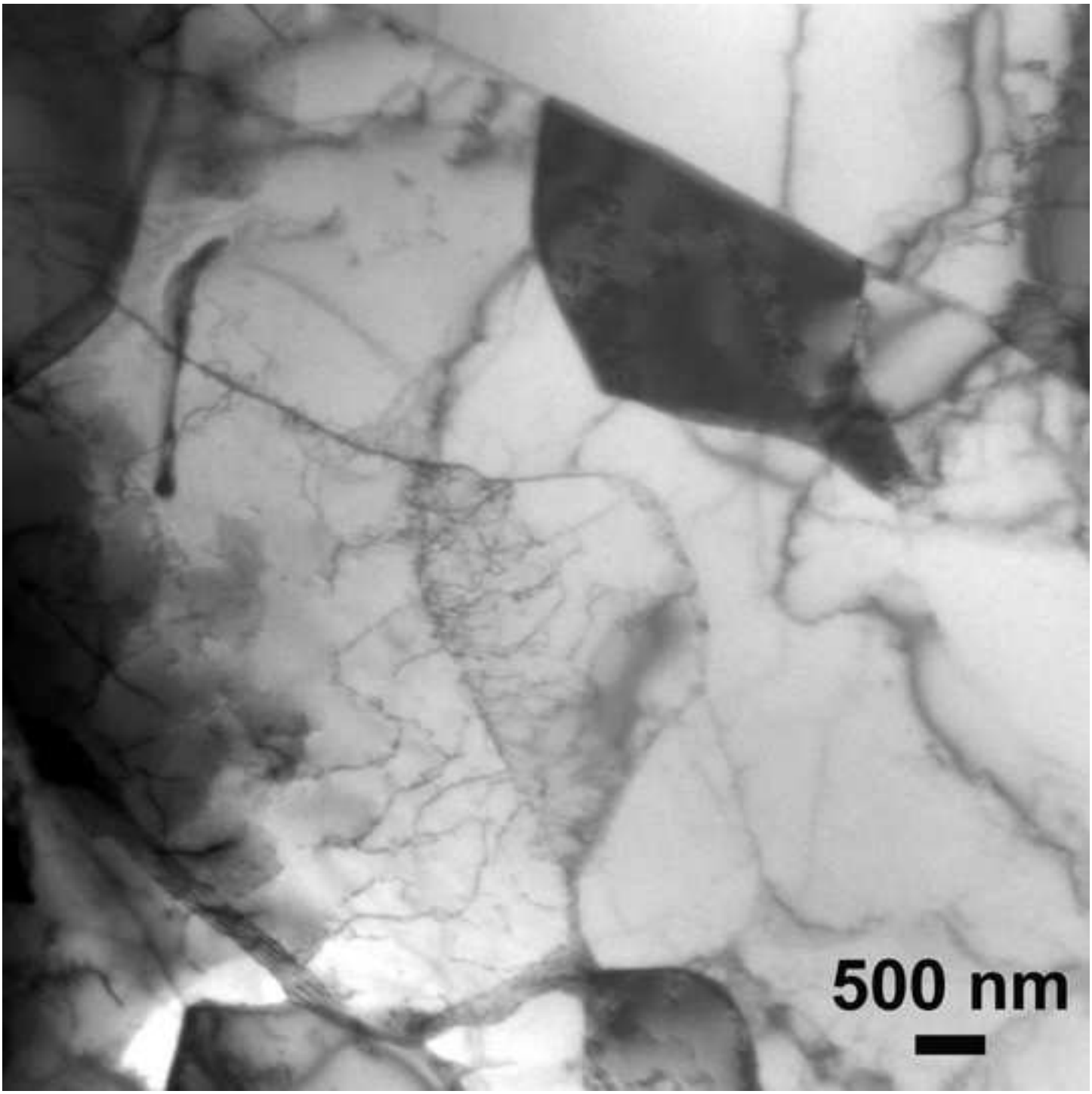

Figure 3a

Click here to download high resolution image

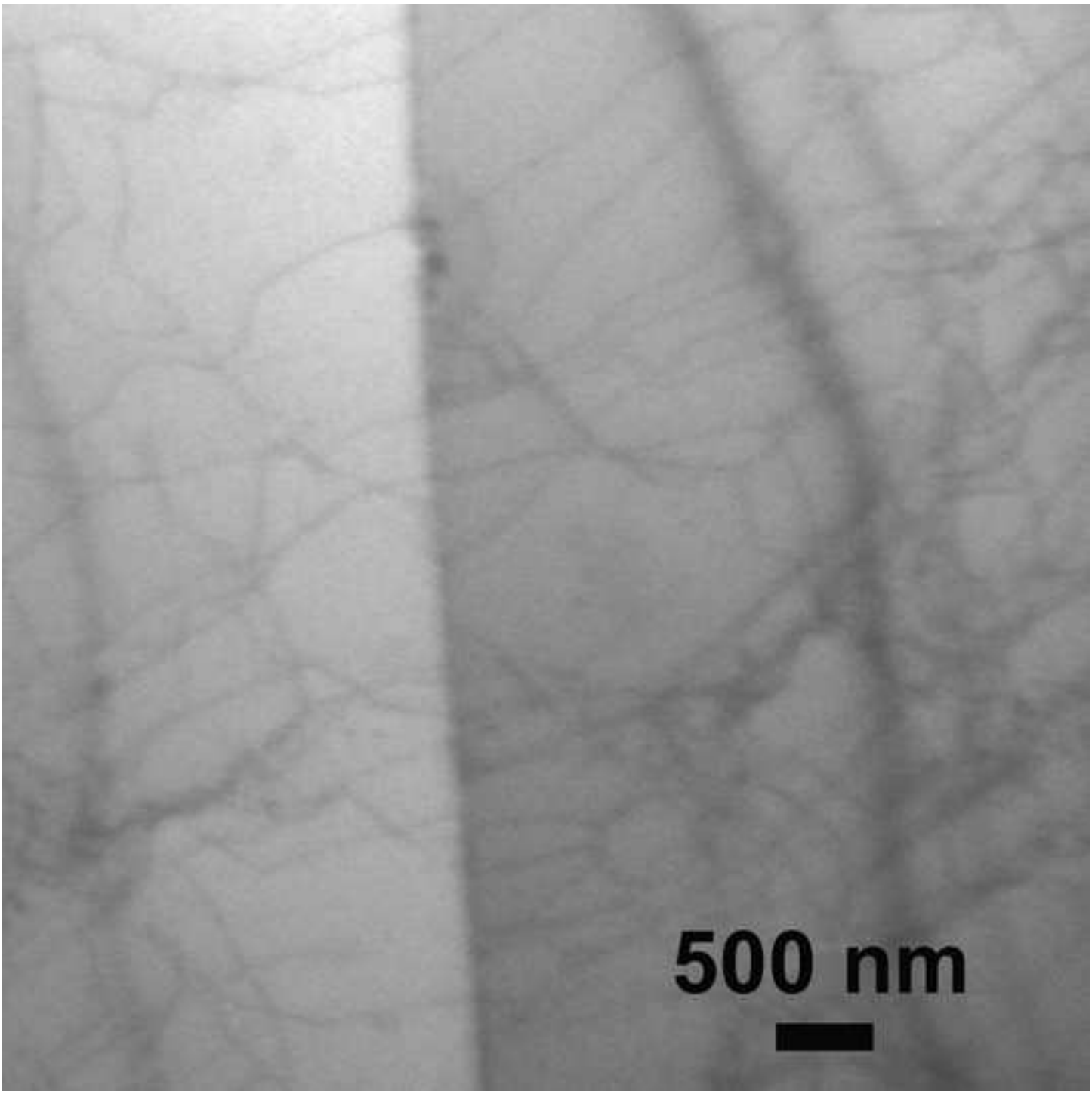

Figure 3b

Click here to download high resolution image

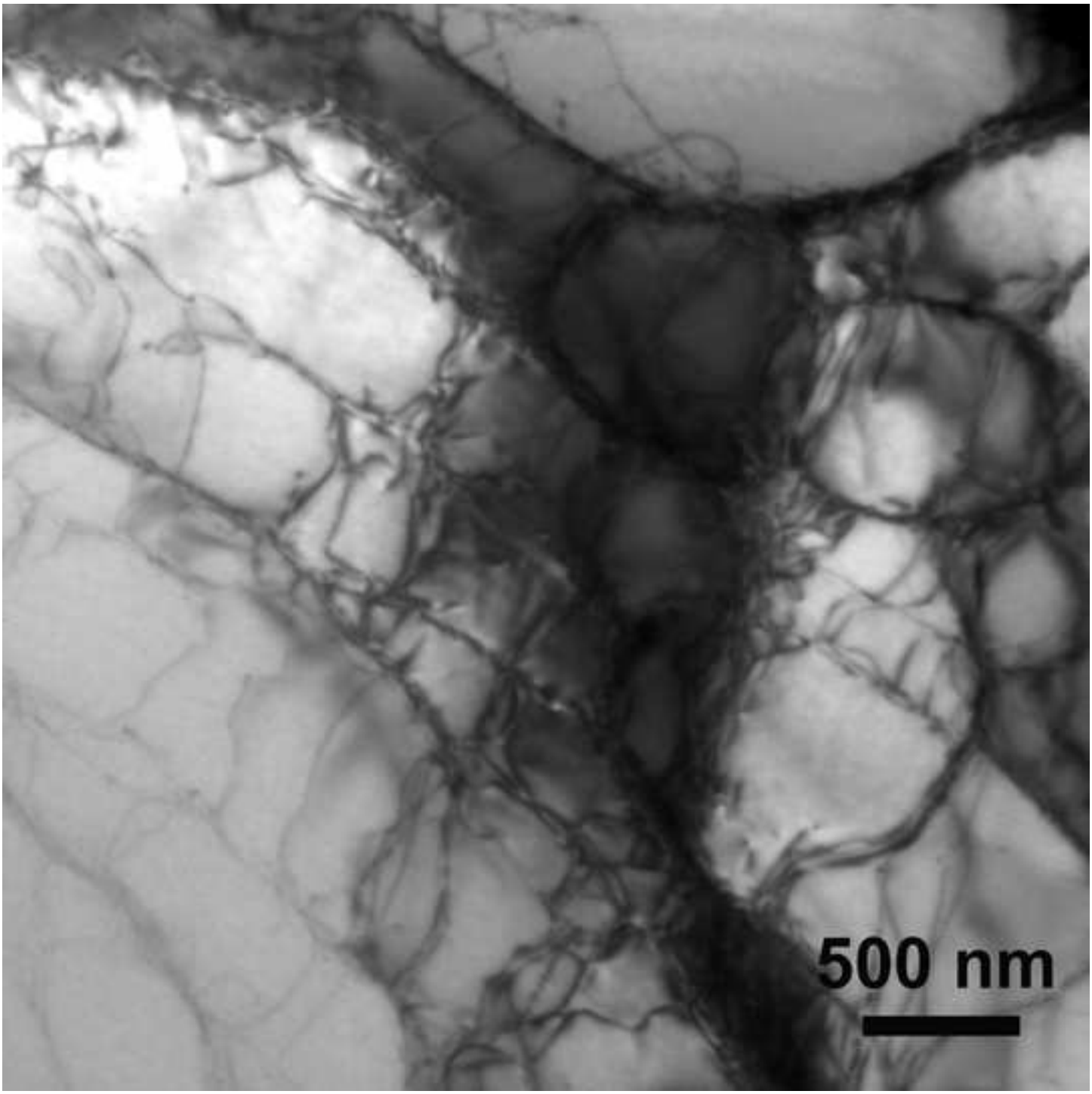

Figure 4

Click here to download high resolution image

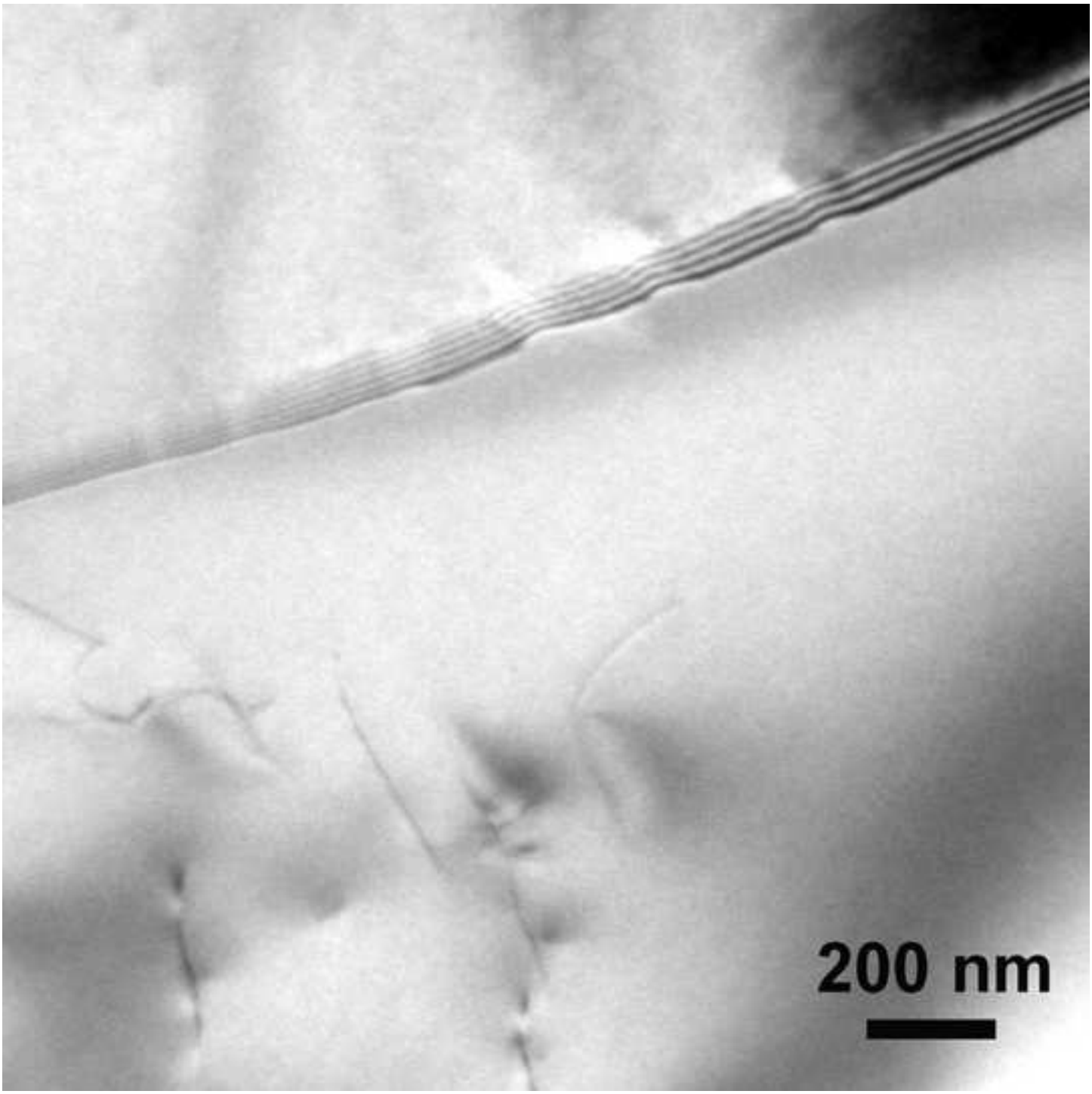

Figure 5

Click here to download high resolution image

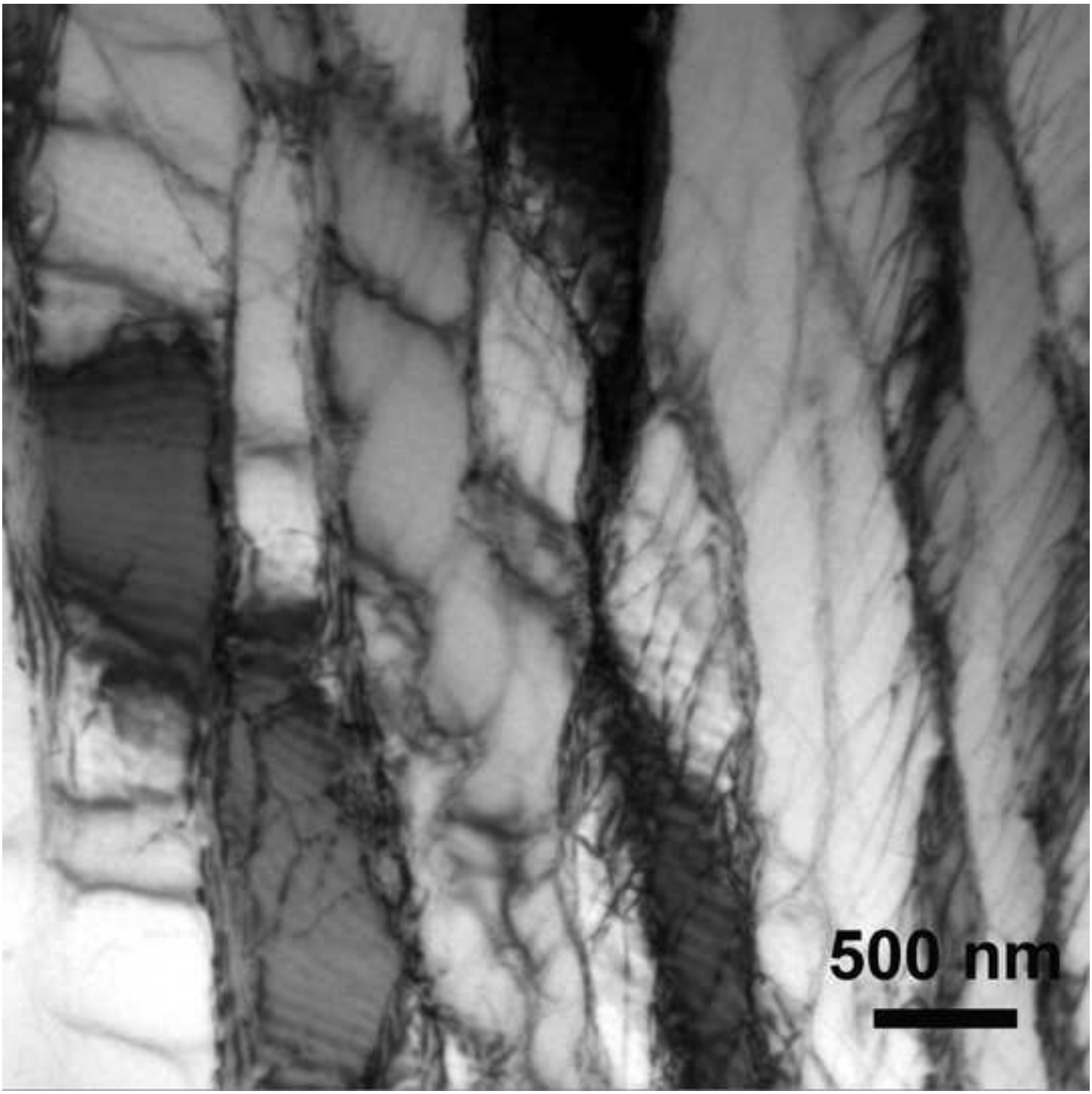

Figure 6a

Click here to download high resolution image

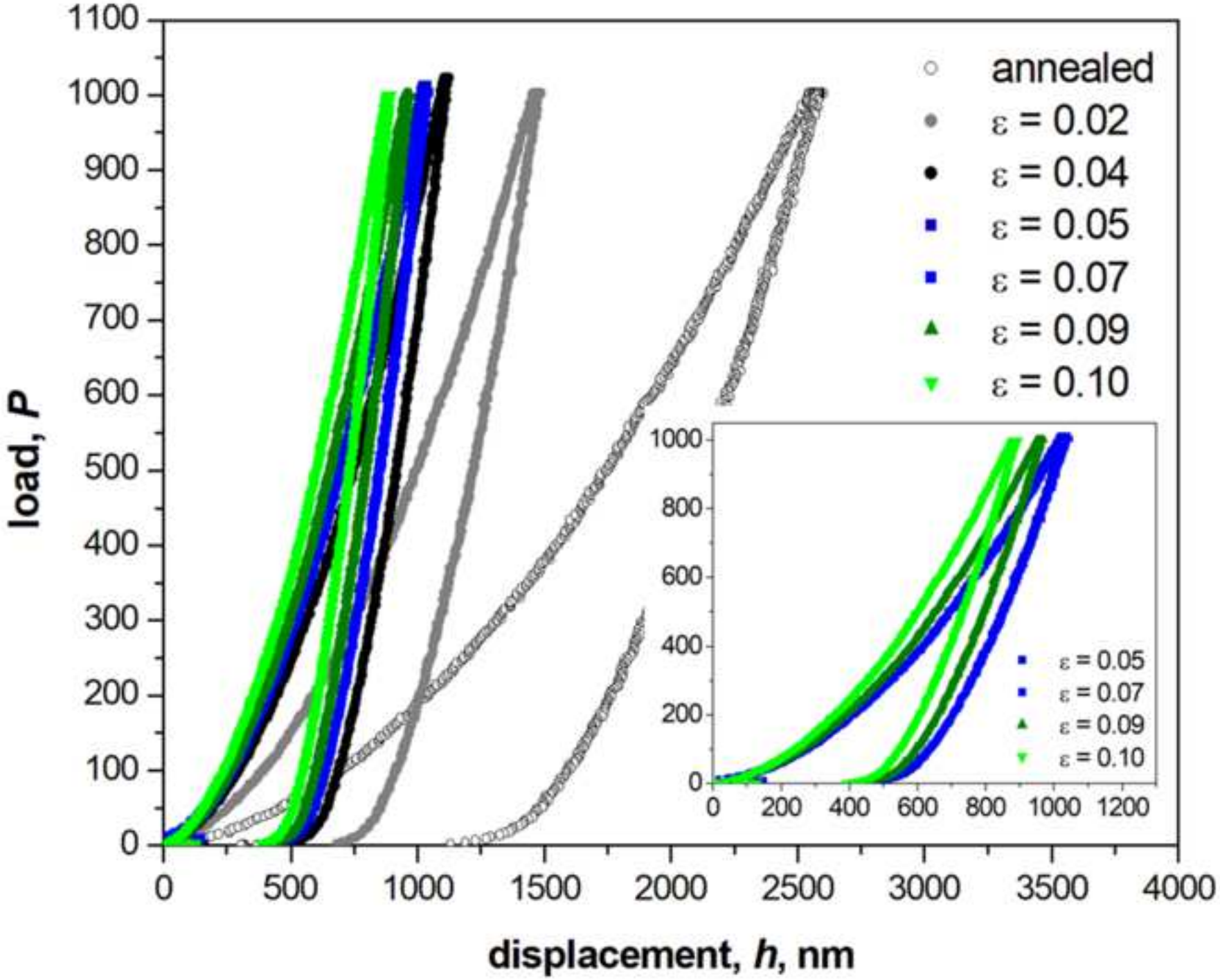

Figure 6b

Click here to download high resolution image

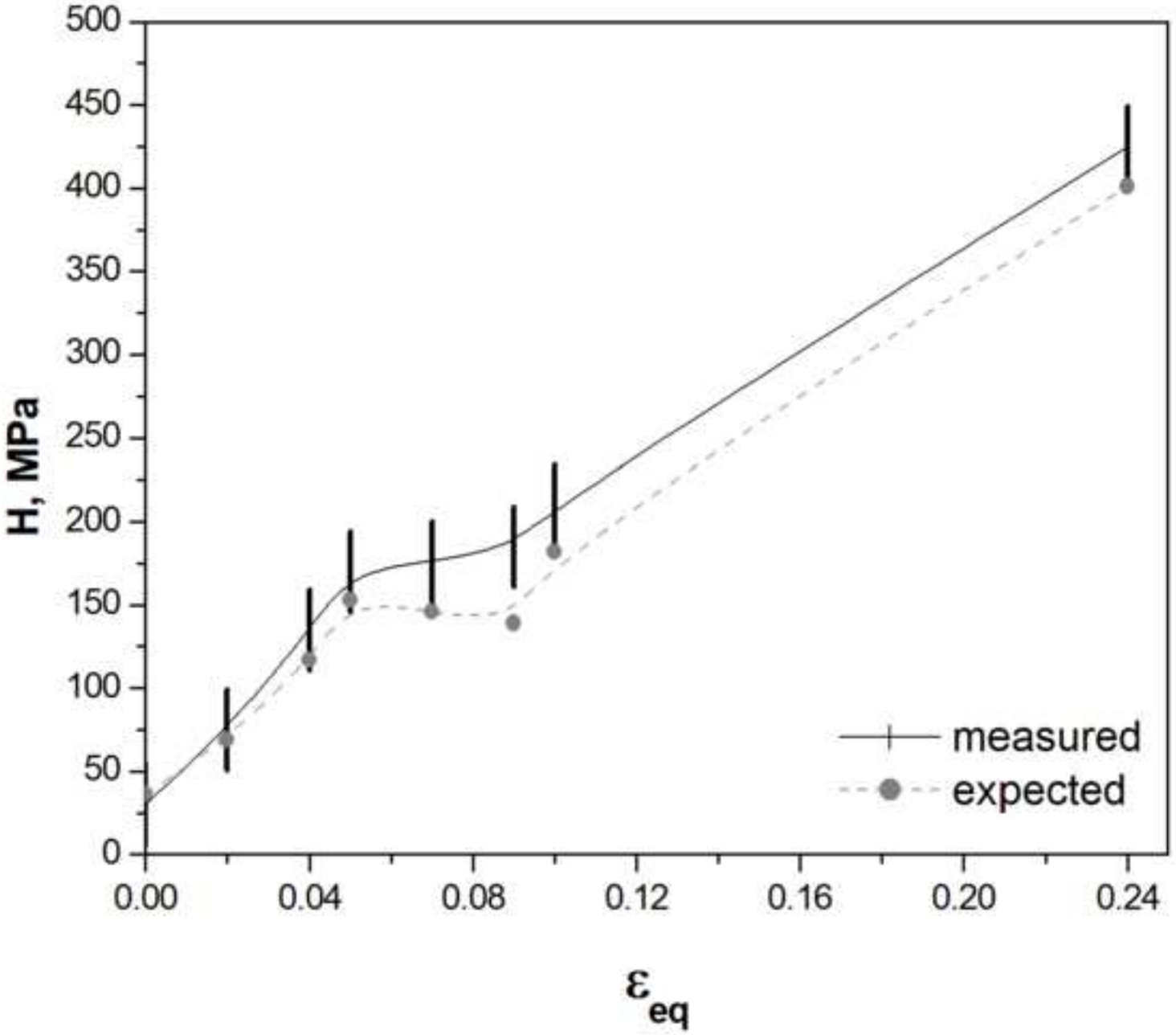

Figure 7

Click here to download high resolution image

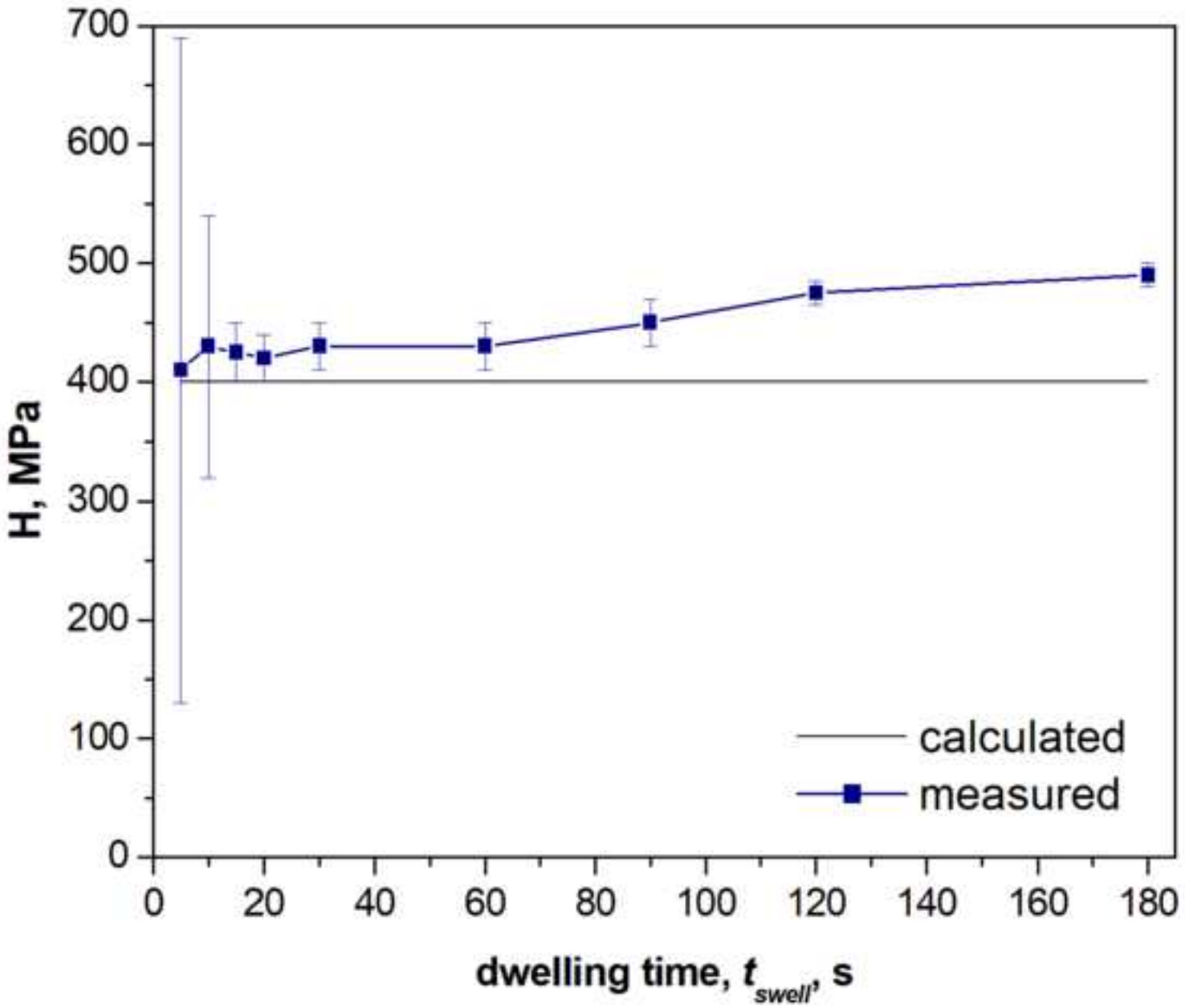

Table 1

	distance to disc center, *r*, mm				
angular rotation, θ, °	~0.3	~0.6	~0.9	~1.2	~1.5
5 (N=1/120)	**0.02**	**0.04**	**0.05**[1]	**0.07**	**0.09**
10 (N=1/72)	0.03	0.06	**0.09**	0.12	0.15
15 (N=1/45)	**0.05**[1]	**0.10**	0.14	0.19	0.24

Table 1. Equivalent strain, ε_{eq}, obtained by HPT N = 1/120, 1/72, and 1/45 turns, and r = 0.3, 0.6, 0.9, 0.12, and 0.15 mm from disc center. Bold values refer to the performed TEM inspections. The ε_{eq}^{1} = 0.05 is the minimum necessary strain to form cell boundaries from TD in 6N-Al.

Table 2

	ε_{eq}							
	0.02 *N*=1/120, *r* = 0.3 mm	0.04 *N*=1/120, *r* = 0.6 mm	0.05 *N*=1/120, *r* = 0.9 mm	0.05 *N*=1/45, *r* = 0.3 mm	0.07 *N*=1/120, *r* = 1.2 mm	0.09a *N*=1/120, *r* = 1.5 mm	0.09b *N*=1/72, *r* = 0.9 mm	0.10 *N*=1/45, *r* = 0.6 mm
ρ_{TD}, 10^{12} m^{-2}	3	18	235	180	160	55	86	62

Table 2. TD density, ρ_{TD}, measured at different strain levels, ε_{eq}, from ε_{eq} = 0.02 to 0.10.

Table 3

	ε_{eq}							
	0.02 *N*=1/120, *r* = 0.3 mm	0.04 *N*=1/120, *r* = 0.6 mm	0.05 *N*=1/120, *r* = 0.9 mm	0.05 *N*=1/45, *r* = 0.3 mm	0.07 *N*=1/120, *r* = 1.2 mm	0.09a *N*=1/120, *r* = 1.5 mm	0.09b *N*=1/72, *r* = 0.9 mm	0.10 *N*=1/45, *r* = 0.6 mm
σ_{TD}, MPa	9	22	26	22	21	13	17	15
$\sigma_{VLAB+LAB}$, MPa	-	-	6	5	9	11	8	14
σ_{HAB}, MPa	-	-	-	-	-	4	5	11
σ_y, MPa	**19**	**32**	**42**	**37**	**40**	**38**	**40**	**50**

Table 3. Proof stress, σ_y, and individual microstructure contributions (σ_{TD}, $\sigma_{VLAB+LAB}$, σ_{HAB}) as determined by Eq. (6a) and Eq. (6b).

graphical abstract

Click here to download high resolution image

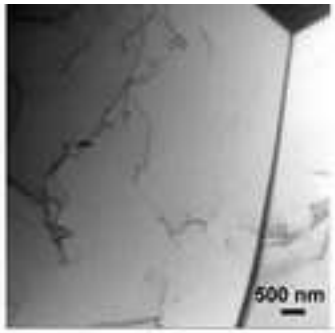

$\varepsilon = 0.02$

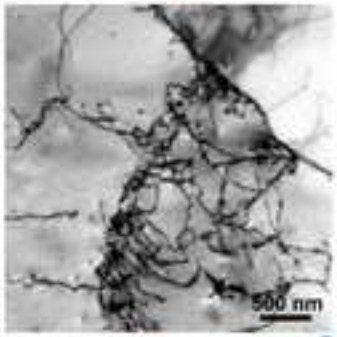

$\varepsilon = 0.04$

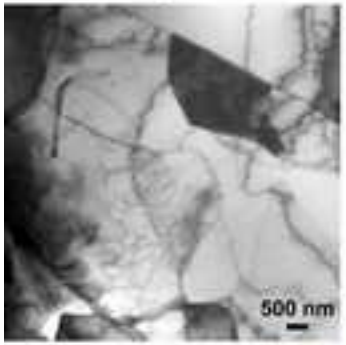

$\varepsilon = 0.05$

$$\sigma_y|_{\varepsilon<0.05} = \sigma_0 + M\alpha Gb\rho_{TD}^{0.5}$$

$$\sigma_y|_{\varepsilon>0.05} = \sigma_0 + M\alpha Gb\rho_{TD}^{0.5} + (\alpha' GbS/4.365)\rho_{VLAB+LAB} + \left(\frac{\alpha' Gb}{4.365}\right)\frac{b\rho_{HAB}}{arctg\,(b/S)}$$

$$\sigma_y|_{\varepsilon>0.20} = \sigma_0 + M\alpha Gb\rho_{TD}^{0.5} + M\alpha G[(3b\theta_{LAB}((1-f_{HAB})/d_{LAB}))^{0.5} + k_{HP}(f_{HAB}/d_{HAB})^{0.5}]$$

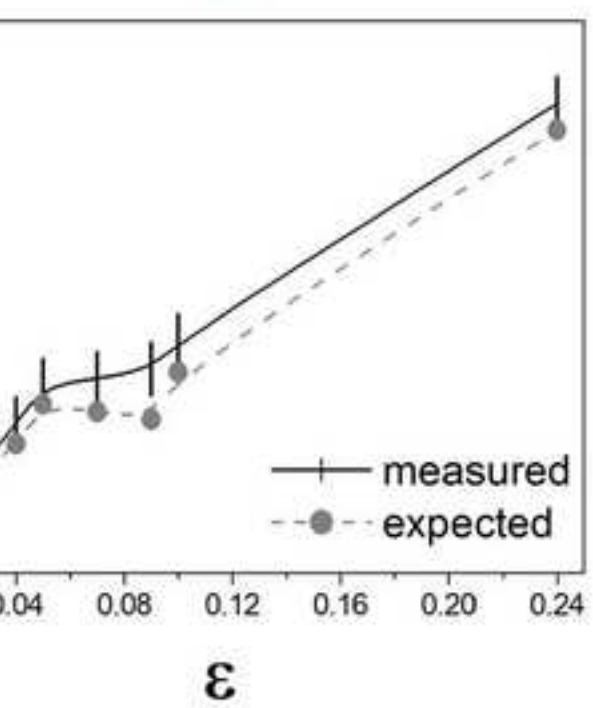

Data in Brief

Click here to download Data in Brief: Data in brief.docx